Introduction to the physical conditions of photo-dissociation regions

Asunción Fuente
Observatorio Astronómico Nacional (OAN-IGN, Spain)

Overview of a PDR

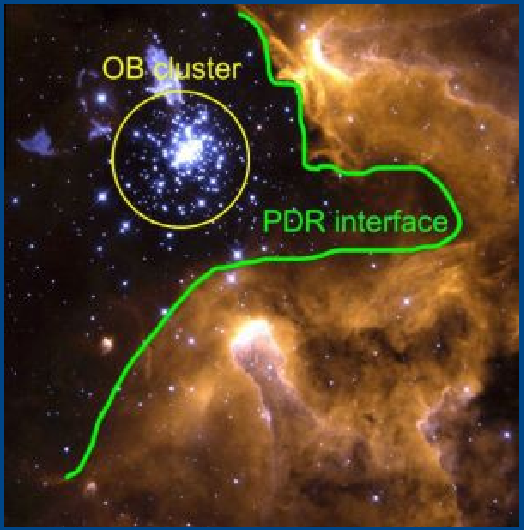

HST-WFPC2
Wolfgang Brandner (JPL/IPAC), Eva K Grebel (Univ. Washington), You-Hua Chu (Univ. illinois) and NASA

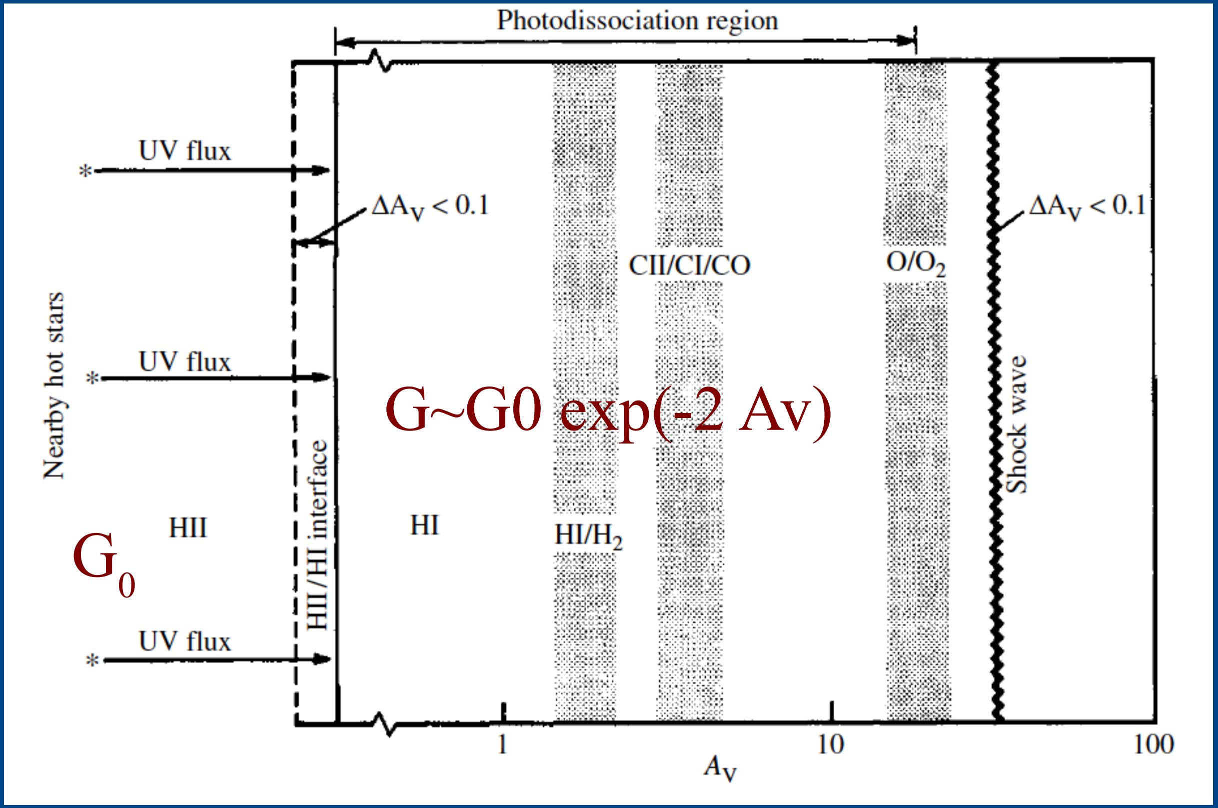

The physical /chemical conditions of a PDR depends on G_0/n and Av

H/H_2 transition at Av~2 mag

C^+/C/CO transition at Av~4 mag

O/O_2 transition at Av~ 20 mag

Heating efficiency

Chemical composition

Why to study PDRs?

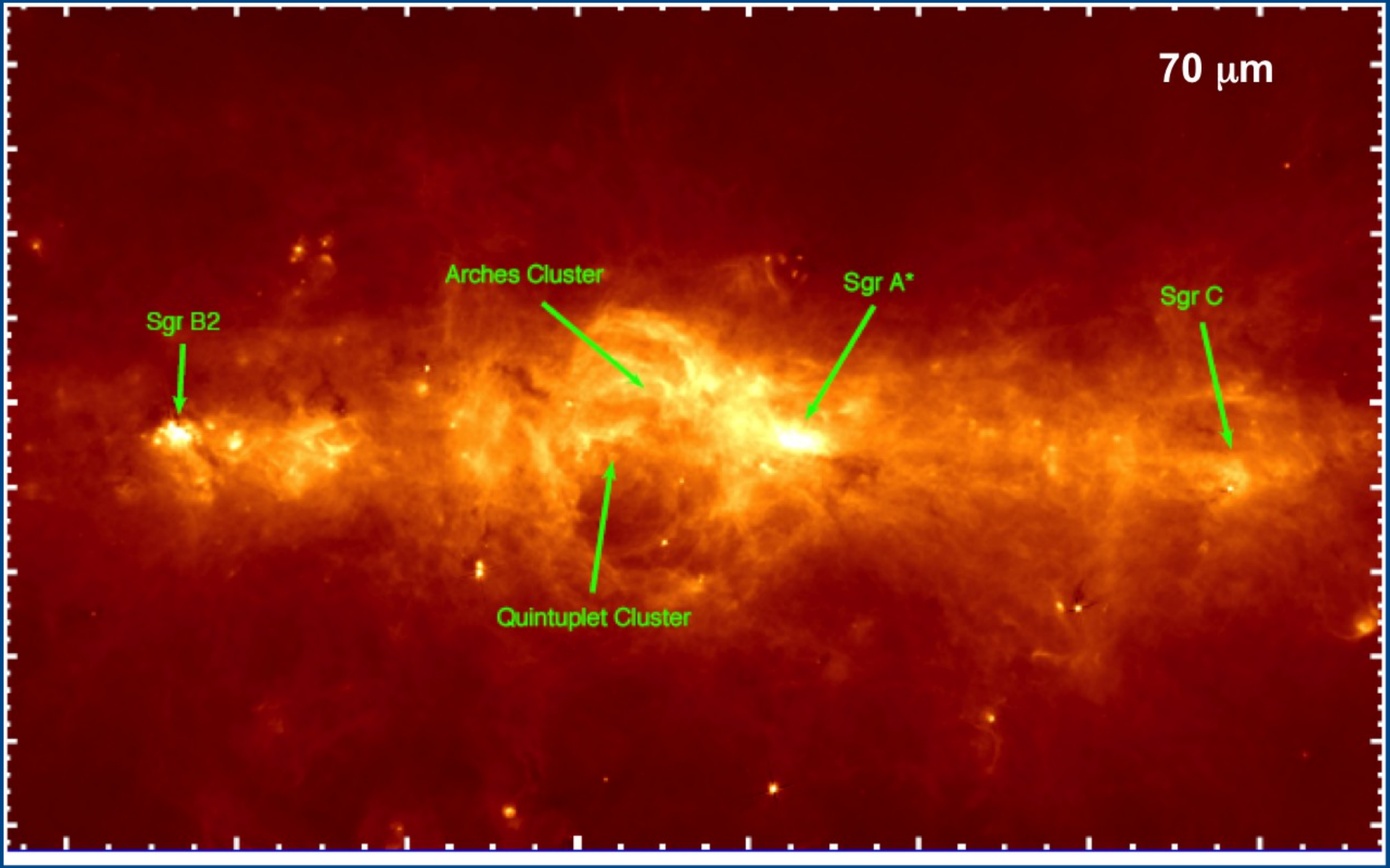

Molinari et al. 2011, ApJ 735, L33

Photodissociation Regions (PDRs)

Photon dominated or photodissociation regions (PDRs) are regions where the FUV radiation dominates the energetic balance and chemistry.

i. The regions close to the O and B stars: HII regions, reflection nebulae, the surface of proto-planetary disks

ii. The surface of molecular clouds

iii. Diffuse clouds

iv. Planetary nebuale

v. The nucleus of starburst galaxies

vi. Distant galaxies?

Mean interstellar field

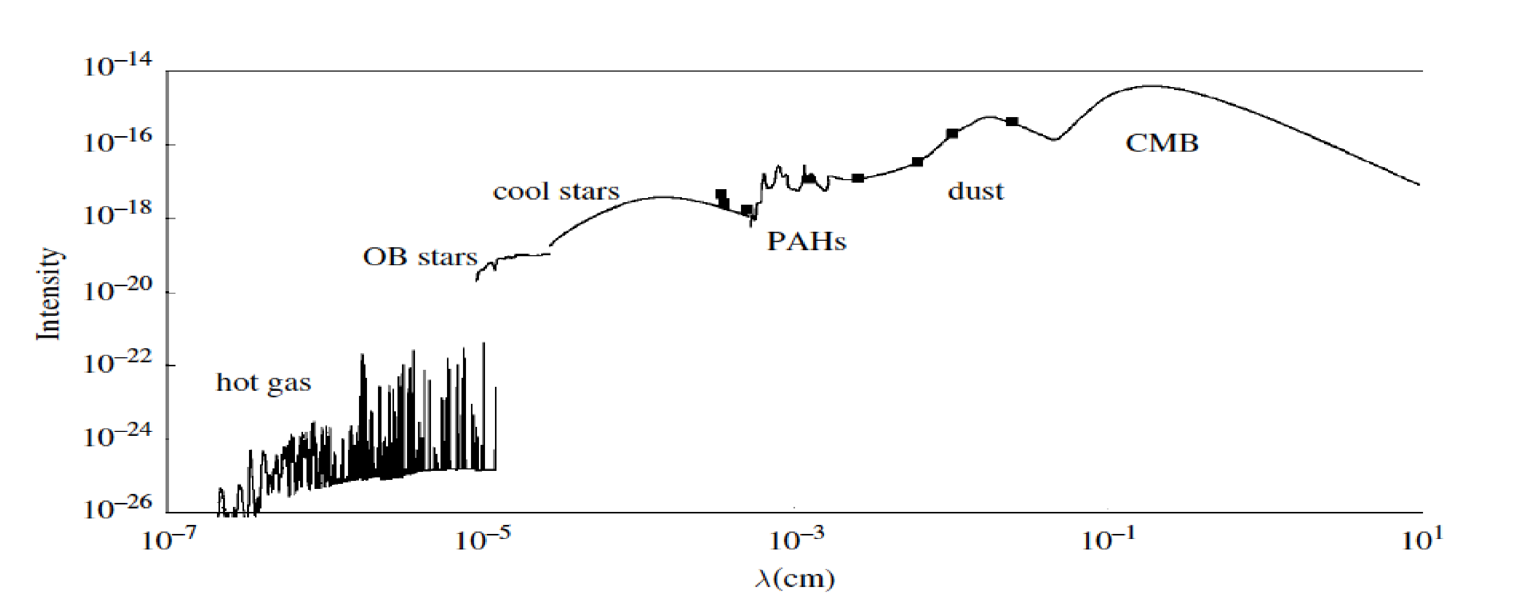

Figure from "The Physics and Chemistry of the Interstellar Medium", A.G.G.M. Tielens, ed Cambridge.

The interstellar radiation field contains contributions from early-type stars, which dominate the FUV (6eV<hν<13.6eV), A stars, which dominates the visible region and late-type stars, which are important at far-red to near-IR. The strength of the FUV interstellar field is expressed in terms of the Habing field = 1.2 x 10^{-4} erg cm^{-2} s^{-1} sr^{-1}=1.6 x 10^{-3} erg cm^{-2} s^{-1}=10^{8} photons cm^{-2} s^{-1}

Mean interstellar field = 1.7 x Habing field = Draine field.

Visual Extinction (Av)

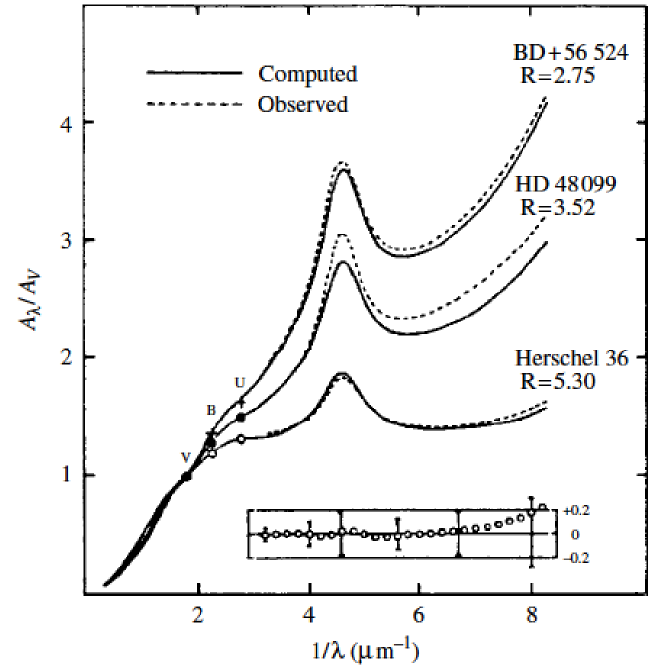

Figure 5.7 Three observed extinction curves are shown as a function of λ^{-1}. These curves show the range in wavelength behavior of the extinction laws in the interstellar medium. The solid lines show, for comparison, the computed parameterized extinction. The insert shows the deviations. Figure courtesy of J. S. Mathis; reprinted with permission from *Ann. Rev. Astron. Astrophys.*, **28**, p. 37, ©1990 by *Ann. Rev.* (www.annualreviews.org).

$$R_V = \frac{A_V}{E(B-V)}$$

R=3.1 diffuse ISM
R=5.0 molecular clouds

$$\frac{N(\mathrm{HI}) + 2N(\mathrm{H_2})}{A_V} = 1.9 \times 10^{21}\,\mathrm{atoms\,cm^{-2}\,magnitude^{-1}}$$

Assuming constant gas/dust ratio ~ 100

Thermal balance

1.- The thermal balance (heating.vs.cooling) determines the gas kinetic temperature.

2.- The evolution of molecular clouds (cloud formation, core collapse) is driven by the equilibrium between the gravitational force and the gas thermal pressure. Gas pressure is determined by the gas kinetic temperature.

Gas Heating

1. UV radiation
   1. Photoionization of C atoms (A_v < 4 mag)
   2. Photodissociation and collisional desexcitation of UV pumped H_2 (A_v < 4 mag)
   3. Photoelectric effect on grains (A_v < 4 mag)
   4. Gas-grain collisions
   5. Collisional desexcitation of the infrared pumped of the OI(63µm) line
2. Cosmic rays
3. Turbulence, shocks, gravity
4. X rays

Photoelectric effect on grains

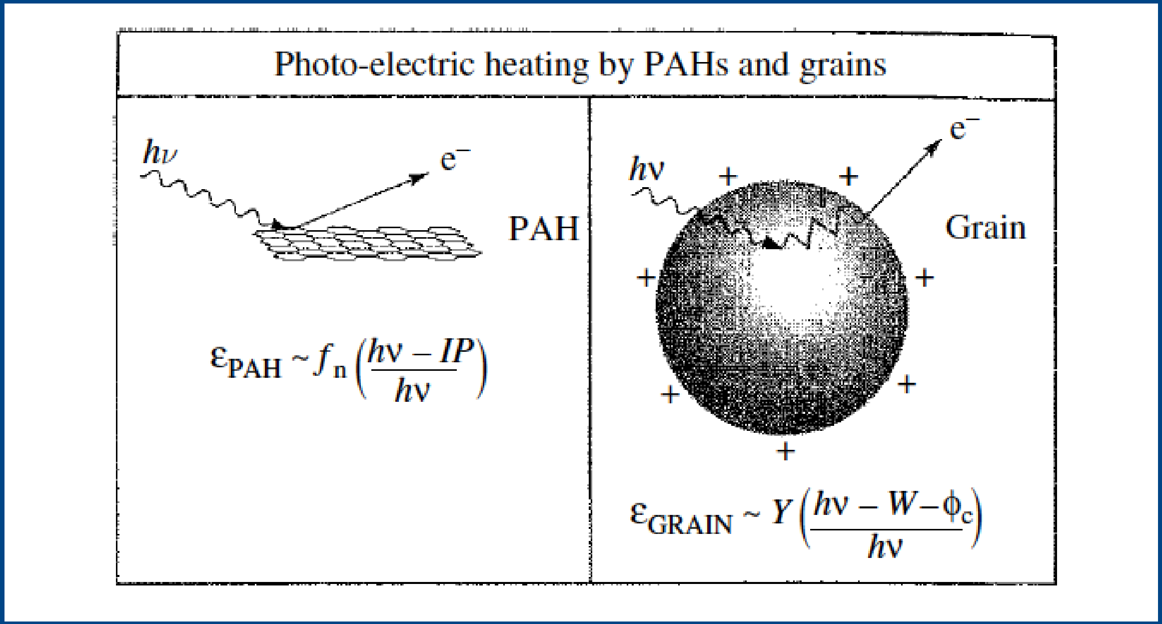

Figure from "The Physics and Chemistry of the Interstellar Medium", A.G.G.M. Tielens, ed Cambridge.

FUV photons (6eV<hυ<13.6eV) absorbed by a grain create energetic e^-. If the energy of these e^- is enough to overcome the work function of the grain and the Coulomb potential (in case of charged grains), the e- is injected into the gas with excess kinetic energy.

Photoelectric effect on grains

$$n\Gamma_{\mathrm{pe}} = 10^{-24}\epsilon n G_0 \,\mathrm{erg\,cm^{-3}\,s^{-1}}.$$

$$\epsilon = \frac{4.87\times10^{-2}}{1+4\times10^{-3}\gamma^{0.73}} + \frac{3.65\times10^{-2}(T/10^4)^{0.7}}{1+2\times10^{-4}\gamma}$$

$\gamma = G_0 T^{1/2}/n_{\mathrm{e}}$ Ratio between photon-ionization and recombination

The efficiency of this process is low (y=0.1): 96 % of the photons energy is absorbed by the grain (grain heating) and only 4% is used in the ejection of e^-

The work funcion of a neutral grain is W = 6 eV. When a photon of 10 eV is absorbed to eject an e^-, only 4 eV are injected to the gas as kinetic energy.

Photoelectric effect on PAHs/grains

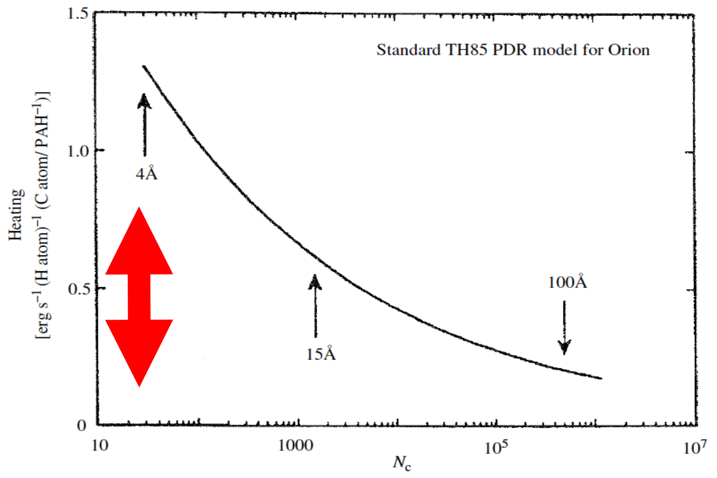

Figure 3.3 The contribution to the photo-electric heating of interstellar gas by PAHs and grains containing different numbers of carbon atoms, N_c. The results of these calculations are presented in such a way that equal areas under the curve correspond to equal contributions to the heating. Typical PAH and grain sizes are indicated.

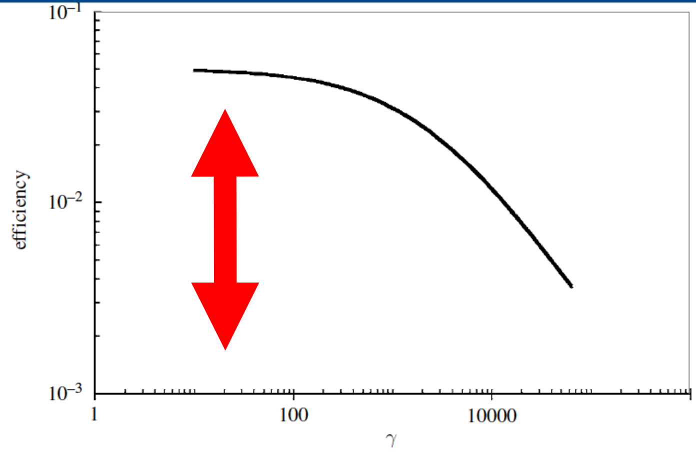

Figure 3.4 The photo-electric heating efficiency as a function of the charging parameter $\gamma \equiv G_0 T^{1/2}/n_e$, which is proportional to the ionization rate over the recombination rate). For low γ, PAHs and grains are neutral and the photo-electric heating is at maximum efficiency. For increasing γ, grains and PAHs charge up and the overall heating efficiency decreases.

The efficiency of this process is low (y=0.1): 96 % of the photons energy is absorbed by the grain (grain heating) and only 4% is used in the ejection of e^-

The efficienty depends on the PAH/grain size and charge. In the case of charged PAH/grains, you need to overcome the Coulomb potential in addition to the work function.

Heating by ionization of C atoms

$$n\,\Gamma_{\rm CI} = 2.2\times10^{-22} f({\rm CI})\mathcal{A}_{\rm C}\, n\, G_0\,\exp[-2.6A_{\rm v}]\,{\rm erg\,cm^{-3}\,s^{-1}}$$

After photo-ionization, the e^- is injected in the gas phase with a kinetic energy 3/2 k T_{ion}. In photodissociation regions, the H atoms cannot be ionized and the first source of e^- is C.

Photodissociation and collisional des-excitation of UV pumped H_2

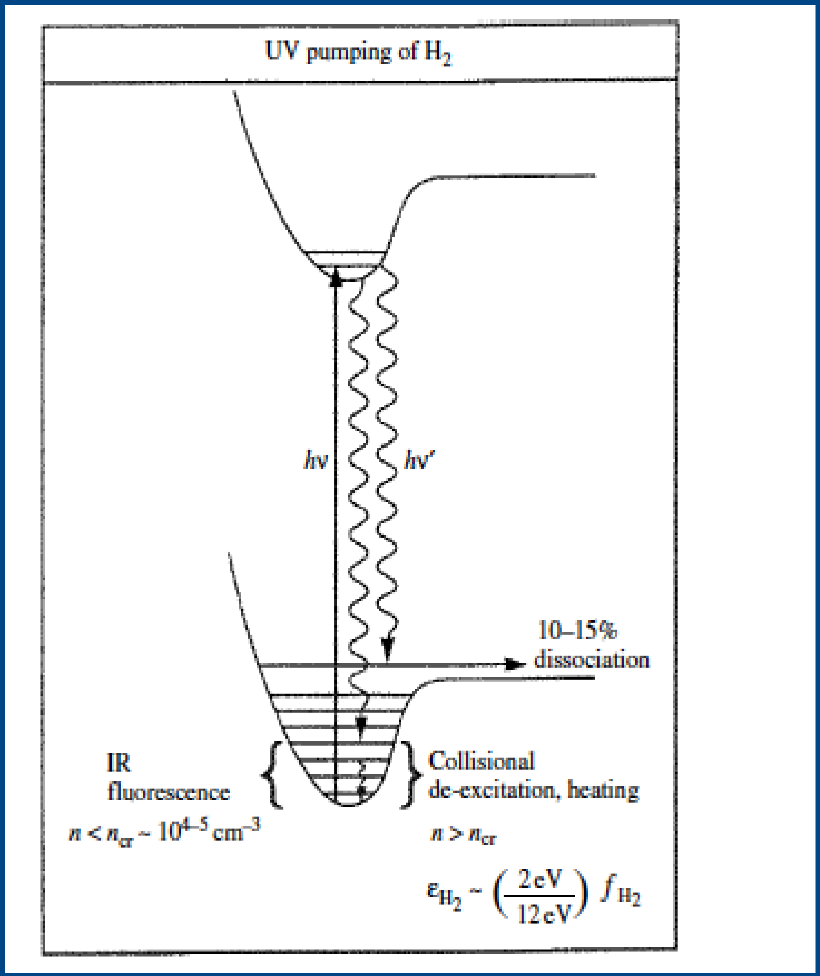

$$n\Gamma_{H_2} \simeq 2.9\times10^{-11}\, n n_H k_d \left[1+\left(\frac{n_{cr}}{n}\right)+\frac{4.4\times10^2\, G_0}{n\, T^{1/2}\exp[-1000/T]}\right]^{-1} \mathrm{erg\ cm^{-3}\ s^{-1}}$$

This heating mechanism can dominate when the density is very high, in this case

$$n\Gamma_{H_2} \simeq 3\times10^{-11}\, n n_H k_d \simeq 10^{-27}\, n n_H\, \mathrm{erg\ cm^{-3}\ s^{-1}}$$

Gas-grain colisions

Γ_{gd}=2.0 10^{-33} n^2 $T^{1/2}$ $(T_d$-T) erg cm^{-3} s^{-1}

When the dust is warmer than the gas, this can be an important heating mechanism. In the contrary case, it is a cooling mechanism. In the limit of high densities, the gas and grains are thermally coupled at the same temperature.

Dust temperature

Dust grains absorbed UV photons, their temperature increase and then irradiate at near-IR and far-IR. The dust temperature is given by the radiative balance

Energy absorbed by the grain = Energy emitted by the grain

$$\Gamma_{\mathrm{abs}} = 4\pi\sigma_{\mathrm{d}} \int_0^\infty Q(\lambda) J(\lambda) \mathrm{d}\lambda,$$

$$\Gamma_{\mathrm{em}} = 4\pi\sigma_{\mathrm{d}} \int_0^\infty Q(\lambda) B(T_{\mathrm{d}}, \lambda) \mathrm{d}\lambda$$

In a PDR, the situation is a bit more complex because you also need to consider the emission from the other dust layers

$$\begin{aligned} 4\pi a^2 \int Q_{\mathrm{abs}}(\nu) \pi B(\nu, T_{\mathrm{d}})\, \mathrm{d}\nu = & \pi a^2 \int Q_{\mathrm{abs}}(\nu)\, F_\star(\nu)\, \exp[-\tau(\nu)]\, \mathrm{d}\nu \\ & + 4\pi a^2 \int Q_{\mathrm{abs}}(\nu) \pi J_{\mathrm{d}}(\nu)\, \mathrm{d}\nu \\ & + 4\pi a^2 \int Q_{\mathrm{abs}}(\nu) \pi B(\nu, T = 2.78K)\, \mathrm{d}\nu, \end{aligned}$$

Dust temperature

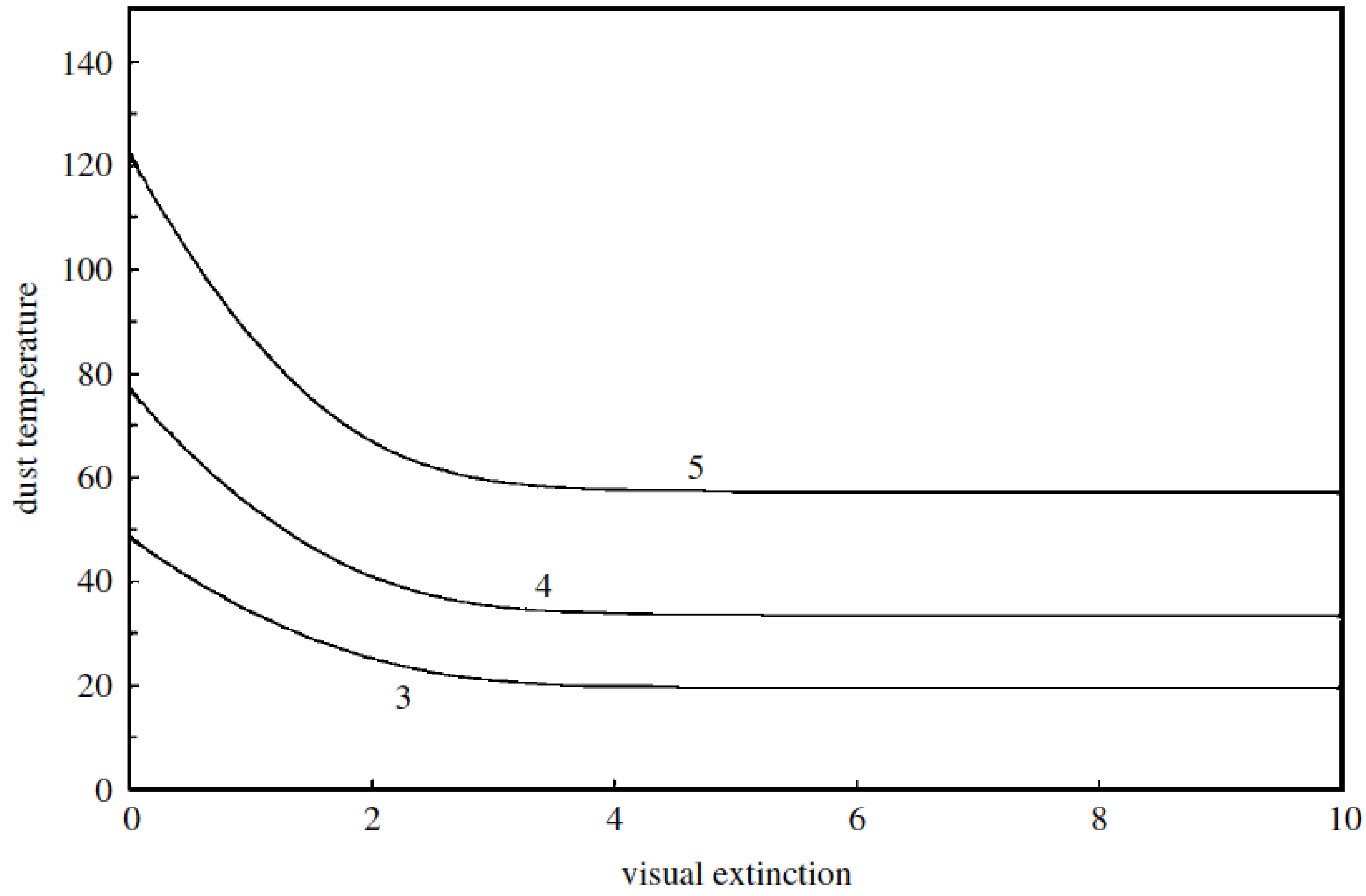

Figure 9.5 The dust temperature as a function of visual extinction in a PDR. The three curves are for a G_0 of 10^3 (3), 10^4 (4), and 10^5 (5).

Cosmic rays

$$n\Gamma_{CR} = 3 \times 10^{-27} n \left[\frac{\zeta_{CR}}{2 \times 10^{-16}}\right] \mathrm{erg\,cm^{-3}\,s^{-1}}.$$

$$\zeta_{CR} \simeq 3 \times 10^{-16}\ \mathrm{s^{-1}}.$$

High energy protons (2 - 10 MeV) ionized tha gas (H_2, He, HD) and inject energetic e^- in the gas.

The efficiency depends on the gas composition, density and ionization degree

Cosmic rays can penetrate much deeper in the molecular clouds (until Av=100 mag) than UV photons (Av<10mag).

Example of Low Density photodissociation region

(Hollenbach, Takahashi & Tielens 1991, ApJ 377, 192)

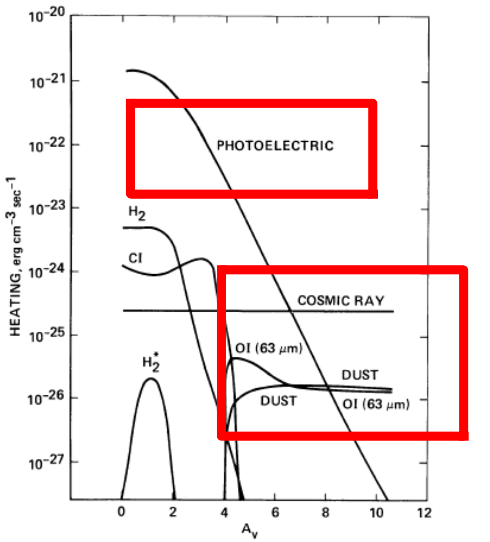

FIG. 1.—Different gas heating terms in the energy balance for the standard model, given as a function of the visual extinction A_v into the cloud. "Photoelectric" refers to the grain photoelectric heating mechanism; "H_2" refers to photodissociation of H_2; "H_2^*" is the collisional de-excitation of FUV–pumped H_2^*; "C I" is the photoionization of atomic carbon; "O I (63 μm)" is the collisional de-excitation of IR-pumped neutral oxygen; "dust" refers to the collisions with warm dust.

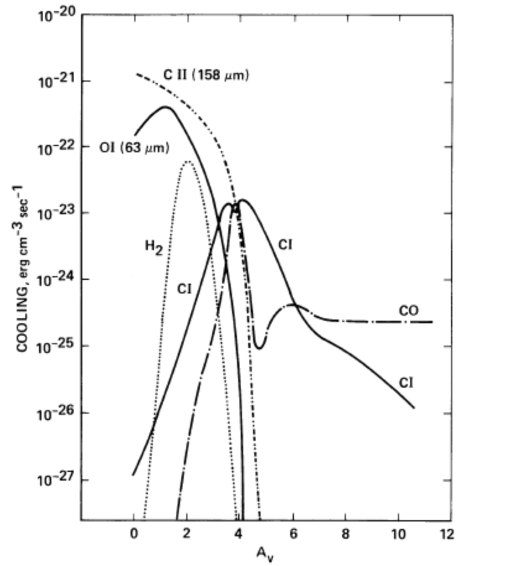

FIG. 2.—Different gas cooling terms in the energy balance for the standard model, given as a function of the visual extinction A_v into the cloud. "C I" is the sum of [C I] 370 μm and [C I] 609 μm; "H_2" and "CO" are the total cooling by rotational and vibrational transitions of these molecules.

TABLE 2

STANDARD MODEL PARAMETERS

Parameter	Standard Model
n_0 (cm^{-3})	1.0 (3)
G_0	1.0 (3)
δv_D (km s^{-1})	1.5
$\mathscr{A}_C$	3.0 (−4)
$\mathscr{A}_O$	5.0 (−4)
$\mathscr{A}_{Si}$	7.9 (−7)
$\mathscr{A}_S$	7.9 (−6)
$\mathscr{A}_{Fe}$	2.5 (−7)
$\mathscr{A}_{Mg}$	1.3 (−6)
δ_d	1.0
δ_{uv}	1.8
k_{uv}	1.8
Y	1.0 (−1)
ϕ_0 (eV)	6.0
T_0 (K)	48.8[a]
$\tau_{100\mu m}$	1.0 (−3)[a]

NOTE.—Numbers in parentheses: see Table 1.

[a] Calculated values according to eqs. (6) and (7).

Gas cooling

When a transition of an atom or molecule is excited collisionally and desexcited radiatively, the gas loose energy and become cooler.

1-Abundant

2.-With transitions that can be collisionally excited with the densities and temperatures of the cloud. $n > n_{cr}$, $T_k \sim Eu\ (K)/2$

3.- It decays radiatively in a short time (A_{ij}).

In the outer layers of the PDR (T>100 K and the gas is mainly atomic), the main coolants are CII (157µm) and OI (63µm and 145µm).

<u>In molecular clouds, the main coolant is CO. In warm regions, water can be an important coolant.</u>

Gas cooling

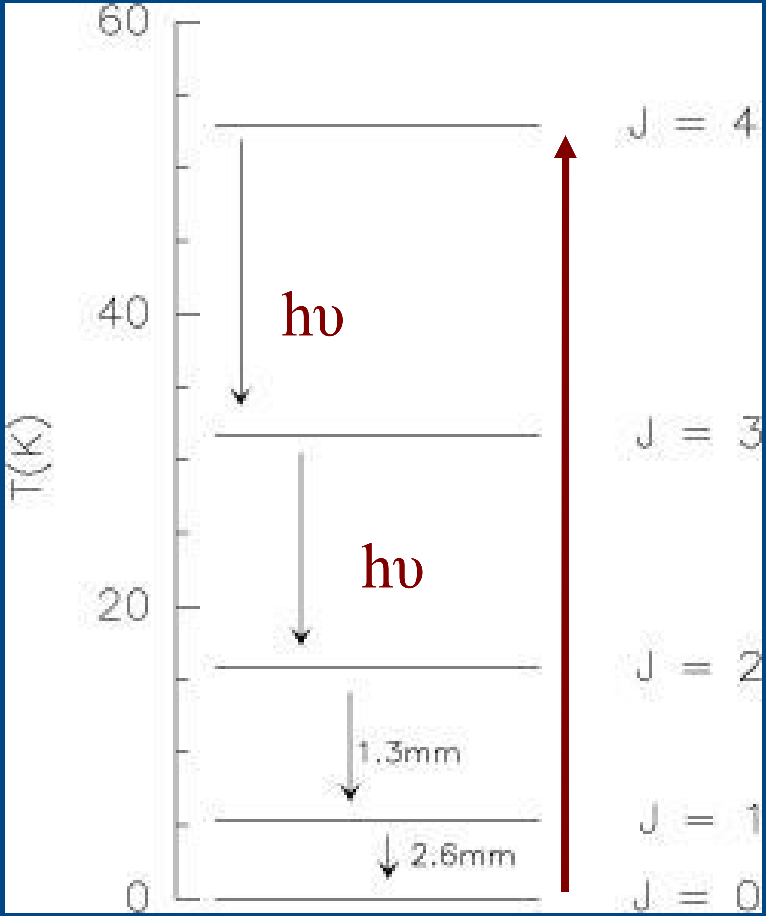

Collisionally excited $n>n_{cr}$
$T_k > E_u/2$ absorbing kinetic energy from the gas

Decay radiatively emitting a photon hυ that escape from the cloud.This photon removes the energy from the gas

Gas cooling (atomic lines)

In the case of optically thin lines, with the two-level aproximation the cooling rate is

$$n^2\,\Lambda = n_{\mathrm{u}} A_{\mathrm{ul}} h\nu_{\mathrm{ul}} = \frac{g_{\mathrm{u}}/g_{\mathrm{l}}\,\exp[-h\nu_{\mathrm{ul}}/kT]}{1 + n_{\mathrm{cr}}/n + g_{\mathrm{u}}/g_{\mathrm{l}}\,\exp[-h\nu_{\mathrm{ul}}/kT]}\,\mathcal{A}_j n\,A_{\mathrm{ul}} h\nu_{\mathrm{ul}}$$

$$n_{\mathrm{cr}} = \frac{A_{\mathrm{ul}}}{\gamma_{\mathrm{ul}}}.$$

Collisional coefficient between the two levels

In the optically thin limit, essentially all collision is followed by a spontaneous desexcitation emitting a photon and

$$n^2\,\Lambda \simeq n^2\,\mathcal{A}_j\,\gamma_{\mathrm{lu}}\,h\nu_{\mathrm{ul}}$$

Gas cooling (CO)

The CO lines are usually optically thick. A modeling of the excitation and radiative transfer is needed to estimate accurately the cooling rate. However, there are some analytical approximations such as

For 10K < T < 60 K y $10^2 < n_{H2} < 10^5$ cm^{-3}

$\Lambda = 1.2\ 10^{-23}\ n_3^{0.4}\ T_{30}^{0.5+(\log n)/2}$ erg cm^{-3} s^{-1}

$n_3 = n_{H2}/10^3$ cm^{-3} y $T_{30} = T/30$ K

(Goldsmith & Langer 1978,ApJ 222,881)

Example of Low Density photodissociation region

(Hollenbach, Takahashi & Tielens 1991, ApJ 377, 192)

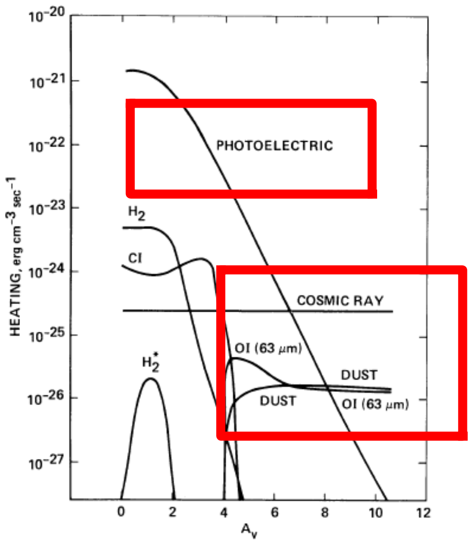

FIG. 1.—Different gas heating terms in the energy balance for the standard model, given as a function of the visual extinction A_v into the cloud. "Photoelectric" refers to the grain photoelectric heating mechanism; "H_2" refers to photodissociation of H_2; "H_2^*" is the collisional de-excitation of FUV–pumped H_2^*; "C I" is the photoionization of atomic carbon; "O I (63 μm)" is the collisional de-excitation of IR-pumped neutral oxygen; "dust" refers to the collisions with warm dust.

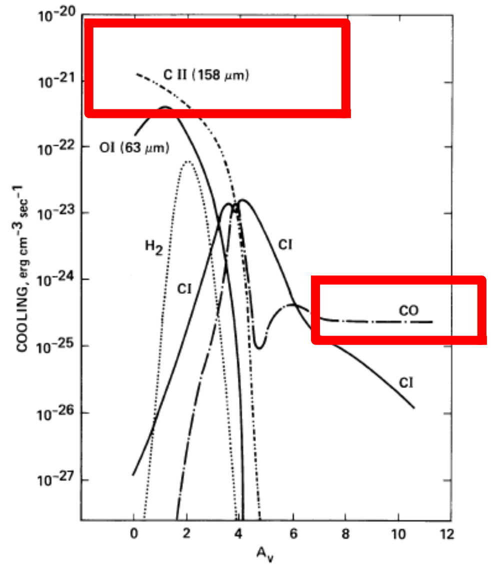

FIG. 2.—Different gas cooling terms in the energy balance for the standard model, given as a function of the visual extinction A_v into the cloud. "C I" is the sum of [C I] 370 μm and [C I] 609 μm; "H_2" and "CO" are the total cooling by rotational and vibrational transitions of these molecules.

TABLE 2

STANDARD MODEL PARAMETERS

Parameter	Standard Model
n_0 (cm^{-3})	1.0 (3)
G_0	1.0 (3)
δv_D (km s^{-1})	1.5
$\mathscr{A}_C$	3.0 (−4)
$\mathscr{A}_O$	5.0 (−4)
$\mathscr{A}_{Si}$	7.9 (−7)
$\mathscr{A}_S$	7.9 (−6)
$\mathscr{A}_{Fe}$	2.5 (−7)
$\mathscr{A}_{Mg}$	1.3 (−6)
δ_d	1.0
δ_{uv}	1.8
k_{uv}	1.8
Y	1.0 (−1)
ϕ_0 (eV)	6.0
T_0 (K)	48.8[a]
$\tau_{100\mu m}$	1.0 (−3)[a]

NOTE.—Numbers in parentheses: see Table 1.

[a] Calculated values according to eqs. (6) and (7).

Example of Dense photodissociation region

(Tielens & Hollenbach, 1985, ApJ 291, 722)

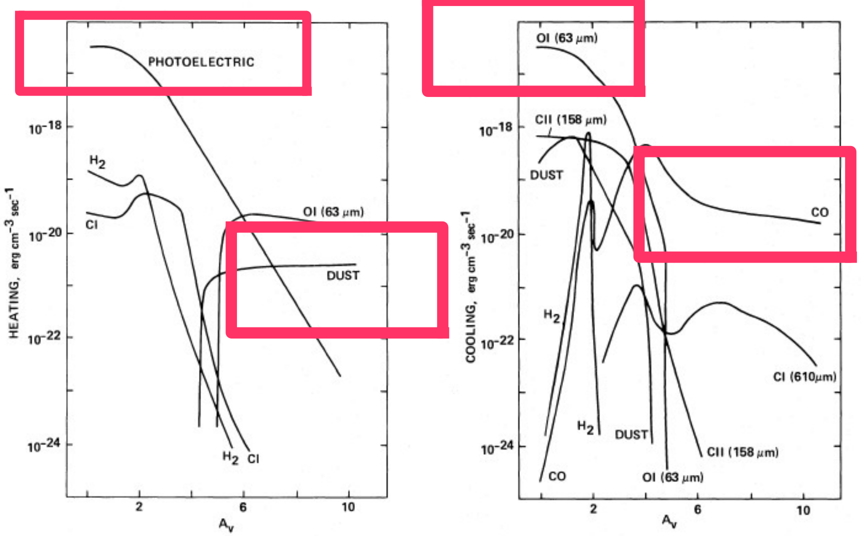

FIG. 8a FIG. 8b

FIG. 8.—(a) The different heating terms in the energy balance are given as a function of visual extinction A_v into the cloud for the standard model (see text). (b) The different cooling terms in the energy balance are shown as a function of visual extinction A_v into the cloud for the standard model (see text).

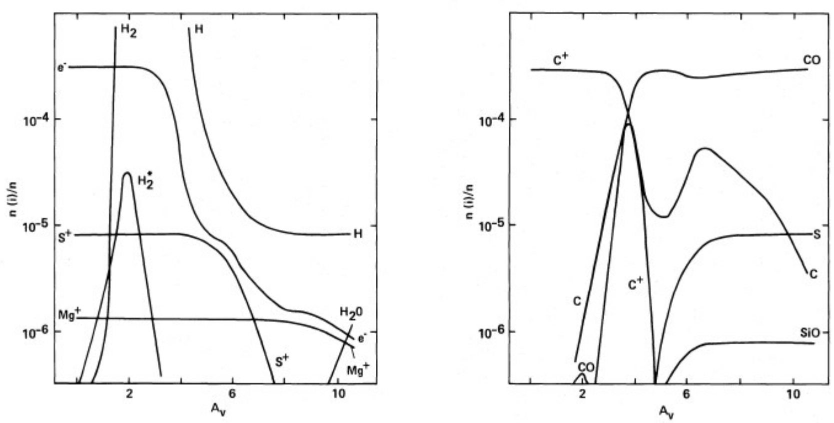

FIG. 9a FIG. 9b

FIG. 9.—The molecular abundances of species i, $n(i)/n_0$, are plotted as a function of visual extinction A_v into the cloud for the standard model

TABLE 2

STANDARD MODEL PARAMETERS

Parameter	Standard Model
n_0 (cm^{-3})	2.3(5)
G_0	1.0(5)
δv_d (km s^{-1})	2.7
$\mathscr{A}_C$	3.0(−4)
$\mathscr{A}_O$	5.0(−4)
$\mathscr{A}_{Si}$	7.9(−7)
$\mathscr{A}_S$	7.9(−6)
$\mathscr{A}_{Fe}$	2.5(−7)
$\mathscr{A}_{Mg}$	1.3(−6)
F_{IR} (ergs cm^{-2} s^{-1})	5.0(2)
T_0 (K)	75
$\tau_{100\ \mu m}$	3.0(−1)
δ_d	1.0
δ_{uv}	1.8
k_{uv}	1.8
Y	1.0(−1)
E_d (eV)	6.0

NOTE.—Numbers in parentheses: 2.3(5) = 2.3 × 10^5.

Gas and Dust temperature

Dense PDR

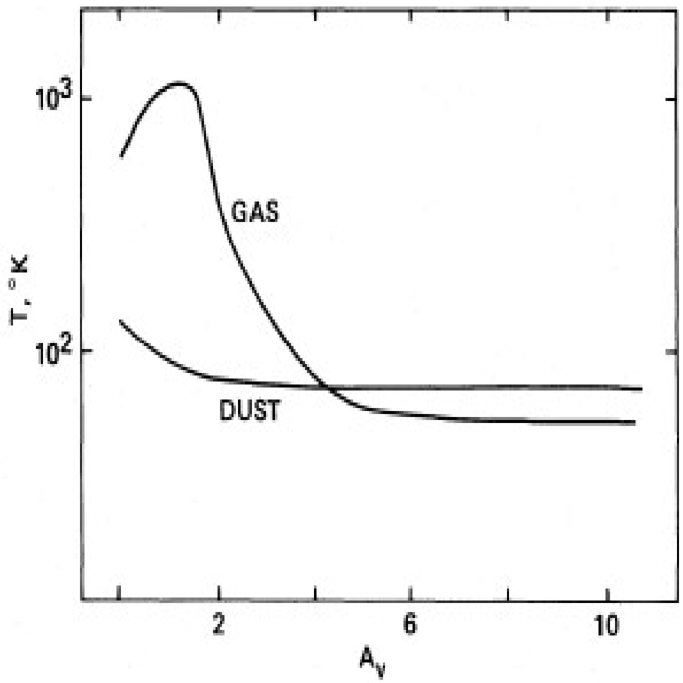

FIG. 7.—The calculated gas and dust temperature in the standard model is plotted as a function of the visual extinction A_v into the cloud.

Low density PDR

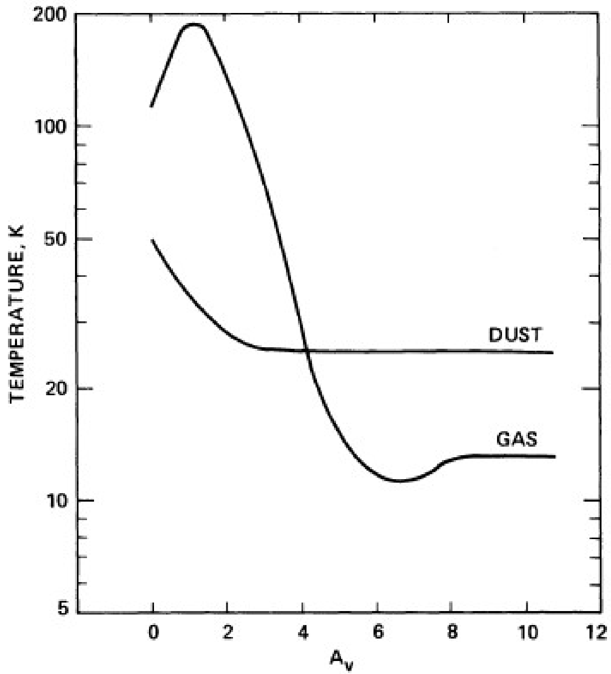

FIG. 3.—Calculated gas and dust temperatures in the standard model (see text), plotted as a function of the visual extinction A_v into the cloud. The grain photoelectric heating heats the gas to higher temperatures than the grains at $A_v \lesssim 4$.

FIR is the domain to study PDRs

i. Dust temperature > 50 K. The thermal dust emission peaks at mid-IR wavelengths.

i. The gas is partially atomic. The most important atomic cooling lines, [CII] 158μm and [OI] 63μm and 145μm, occurs in the FIR domain.

i. The most intense molecular lines in PDRs, mid- and high-J CO rotational lines, also at FIR and mid-IR frequencies.

Comparison with observations

The goal of PDR models is to derive the physical conditions of the PDR (n, G_0, T) from observations. FIR lines are adequate, because they tell us about the energetic balance.

Model Name	Authors
Cloudy	G. J. Ferland, P. van Hoof, N. P. Abel, G. Shaw (Ferland et al. 1998; Abel et al. 2005; Shaw et al. 2005)
COSTAR	I. Kamp, F. Bertoldi, G.-J. van Zadelhoff (Kamp & Bertoldi 2000; Kamp & van Zadelhoff 2001)
HTBKW	D. Hollenbach, A. G. G. M. Tielens, M. G. Burton, M. J. Kaufman, M. G. Wolfire (Tielens & Hollenbach 1985; Kaufman et al. 1999; Wolfire et al. 2003)
KOSMA-τ	H. Störzer, J. Stutzki, A. Sternberg (Störzer et al. 1996), B. Köster, M. Zielinsky, U. Leuenhagen Bensch et al. (2003), Röllig et al. (2006)
Lee96mod	H.-H. Lee, E. Herbst, G. Pineau des Forêts, E. Roueff, J. Le Bourlot, O. Morata (Lee et al. 1996)
Leiden	J. Black, E. van Dishoeck, D. Jansen and B. Jonkheid (Black & van Dishoeck 1987; van Dishoeck & Black 1988; Jansen et al. 1995)
Meijerink	R. Meijerink, M. Spaans (Meijerink & Spaans 2005)
Meudon	J. Le Bourlot, E. Roueff, F. Le Petit (Le Petit et al. 2005, 2002; Le Bourlot et al. 1993)
Sternberg	A. Sternberg, A. Dalgarno (Sternberg & Dalgarno 1989, 1995; Boger & Sternberg 2005)
UCL_PDR	S. Viti, W.-F. Thi, T. Bell (Taylor et al. 1993; Papadopoulos et al. 2002; Bell et al. 2005)

PDR diagnostic model diagrams

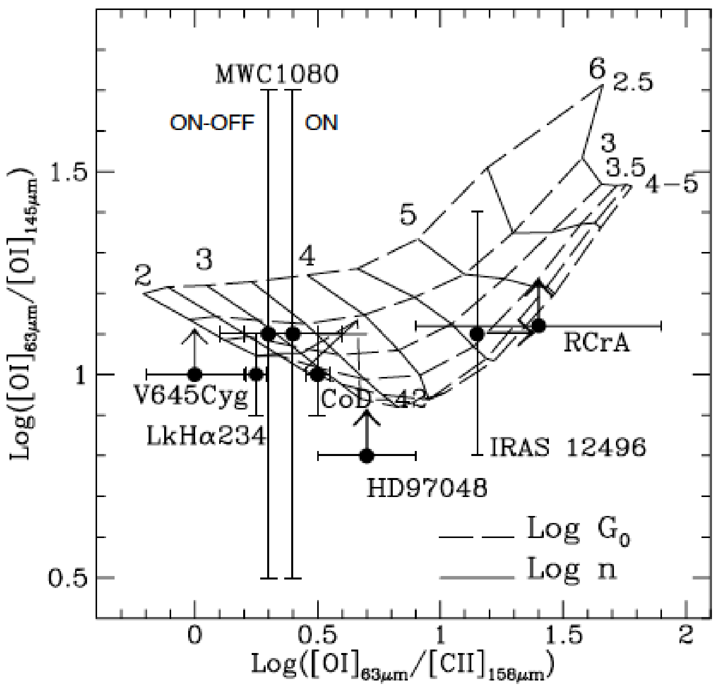

Fig. 4. Observed line ratios superimposed to PDR model (see text).

Lorenzetti et al (1999) used the [OI]63μm/[CII]157μm and [OI]63μm/[OI]145μm intensity ratios to derive the physical conditions of the PDRs associated with Herbig Ae/Be stars based on ISO data.

PDR diagnostic model diagrams

PDR diagmostic diagrams are useful to derive global properties. If the main heating mechanism is the photoelectric effect, heating efficiency depends on the grain charge which is itself governed by the paramter $G_0 T^{1/2} / n_e$.

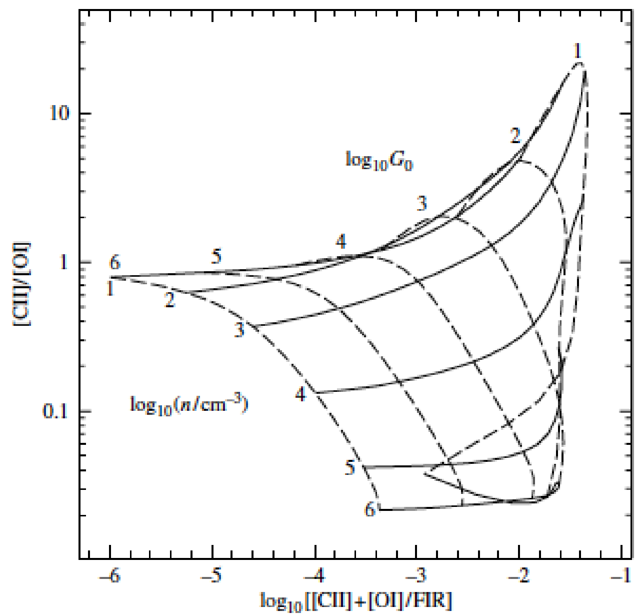

Figure 9.9 A diagnostic diagram for PDRs based on the observed intensity ratio of the [CII] 158 µm and [OI] 63 µm lines and the overall cooling efficiency. The lines present the results of detailed model calculations for different densities and incident FUV fields. Figure kindly provided by M. J. Kaufman; derived from the models described in M. J. Kaufman, M. G. Wolfire, D. Hollenbach, and M.L. Luhman, 1999, *Ap. J.*, **527**, p. 795.

$$\frac{F_{\mathrm{OI}} + F_{\mathrm{CII}}}{2F_{\mathrm{IR}}}$$

Gas heating efficiency

Since the [CII] 158 μm and [OI 63 μm lines have different critical densities, their intensity ratio is a good measure of the density.

PDR diagnostic model diagrams

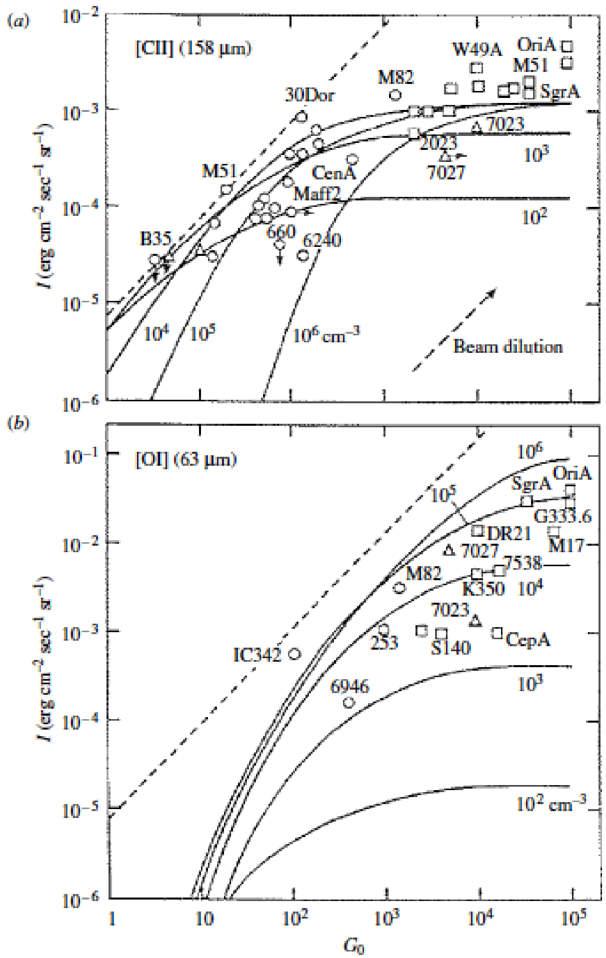

Figure 9.11 Comparison of observed and calculated line intensities of the [CII] 158 µm (*a*) and [OI] 63 µm (*b*) lines as a function of the incident FUV field, G_0. Symbols represent PDRs associated with HII regions (squares), reflection nebulae, dark clouds, and planetary nebulae (triangles), and galactic nuclei (circles). The models are labeled by their density. The dashed line indicates an efficiency of 3% in converting incident FUV energy into gas cooling. Figure reproduced with permission from D. Hollenbach, T. Takahashi, and A. G. G. M. Tielens, 1991, *Ap. J.*, **377**, p. 192.

PDRs diagnostic diagrams based on line intensities have the problem of the unknown beam filling factor. Ratios between the intensities of two lines or between lines and FIR continuum are preferred.

What is an HII region?

A massive star (O & B type) radiates enough **UV photons** with **energies E > 13.6 eV** that ionize the surrounding gas and generate an **HII region**

… radiates **photons** with energies **6 < E < 13.6 eV** that **dissociate H_2** and **CO** molecules and generate a **PDR (phodon-dominated region)**.

	Size (pc)	Density (cm^{-3})	Ionized mass ($M_\odot$)
Hypercompact	<0.03	$>10^6$	10^{-3}
Ultracompact	<0.1	$>10^4$	10^{-2}
Compact	<0.5	$>10^3$	1
Classic	10	100	10^5
Giant	100	30	$10^3 – 10^6$
Supergiant	>100	10	$10^6 – 10^8$

Kurtz (2005)

Size of the HII region, related to …

the number of ionizing photons

the density of the surrounding gas

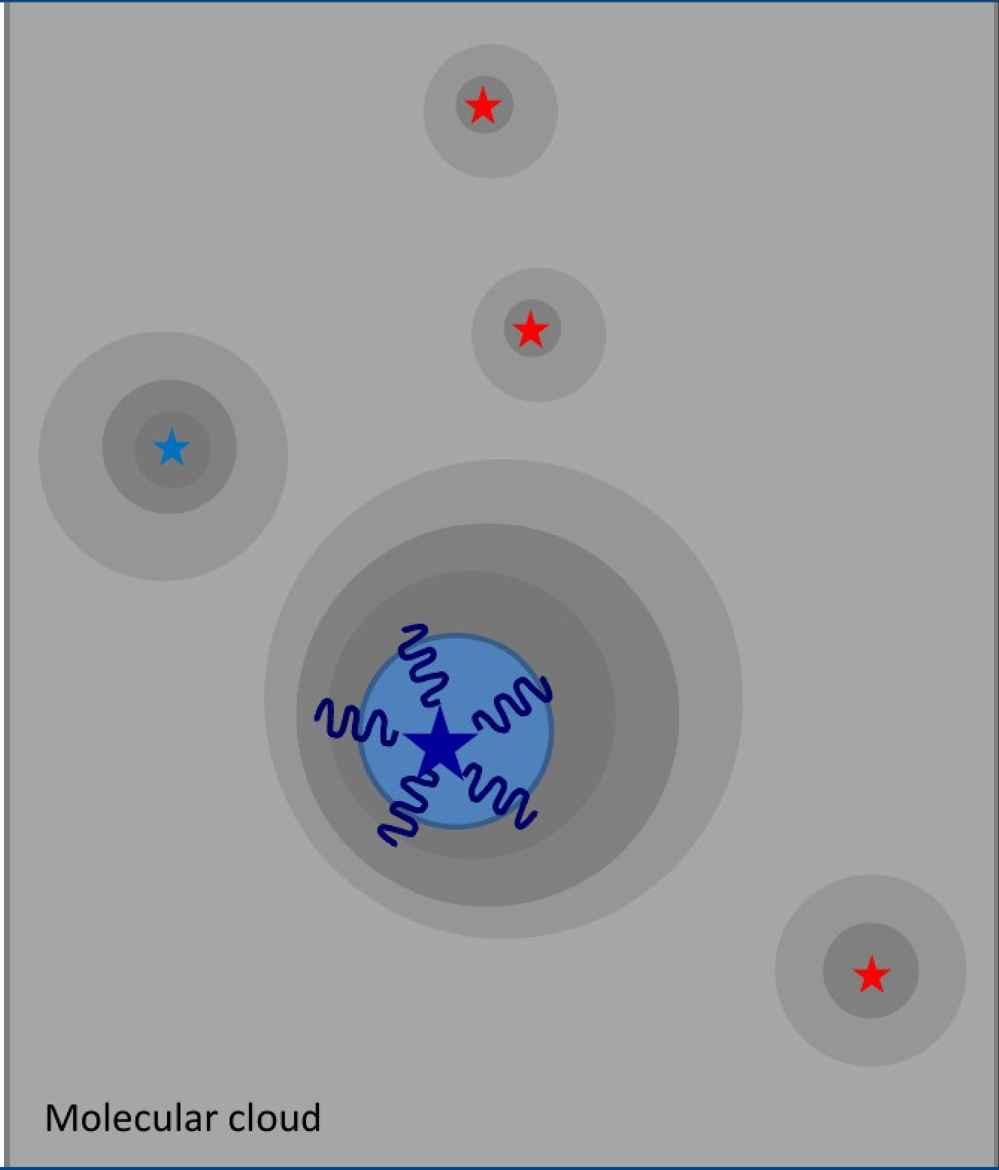

Extreme photon-dominated regions

A massive star (O & B type) radiates enough **UV photons** with **energies E > 13.6 eV** that ionize the surrounding gas and generate an **HII region**

... radiates **photons** with energies **6 < E < 13.6 eV** that **dissociate H_2** and **CO** molecules and generate a **PDR (phodon-dominated region).**

- ***Link*** between HII region and molecular cloud
- Chemistry dominated by ***FUV photons***
- Structure (chemistry/physics) determined by
  - n, ***gas density***
  - G_0, ***incident flux***

G_0, incident flux: from 1.7 (interstellar radiation field) to 10^6 (close to high-mass stars)
with $G_0 \approx 1.6 \cdot 10^{-3}$ erg cm^{-2} s^{-1} (Habing 1968)

Hollenbach & Tielens (1997)

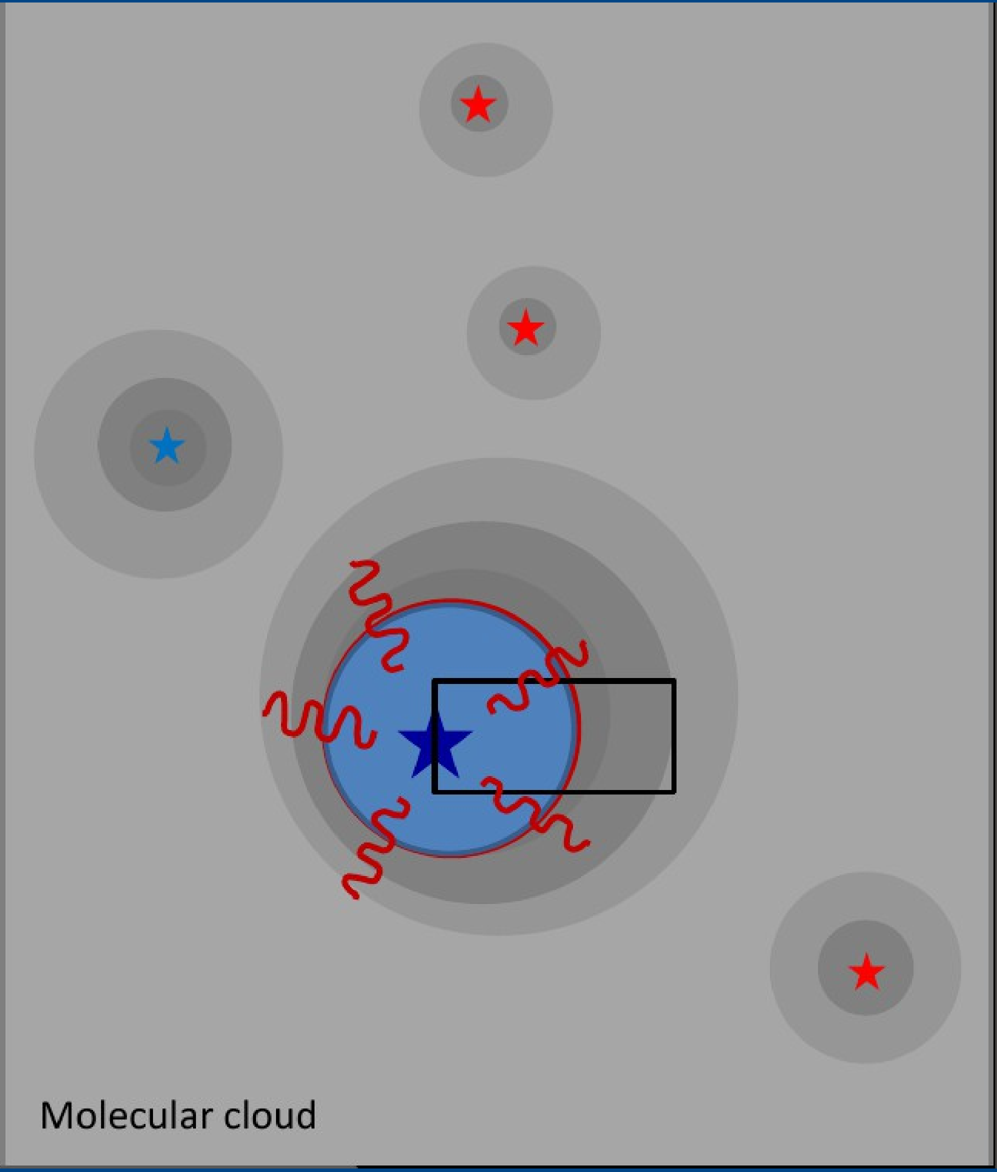

PAHs

PAHs influence the physics and chemistry of PDRs:

1.- Heating the gas by the photoelectric effect

2.- UV photons ionizes PAHs increasing the number of e-

3.- Photochemistry

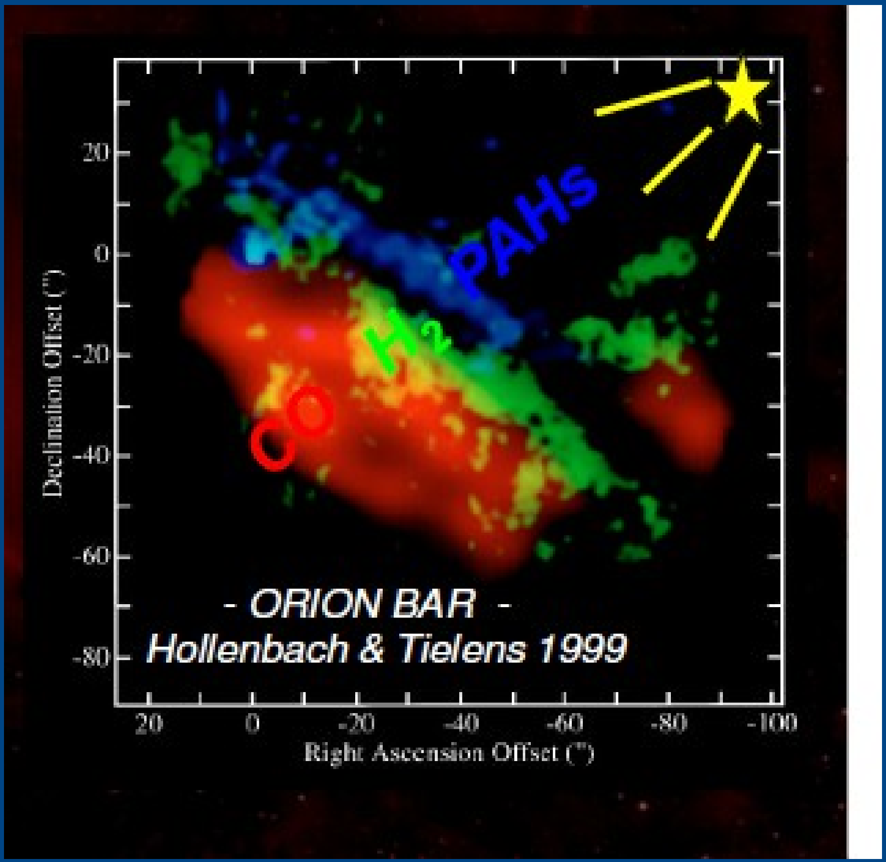

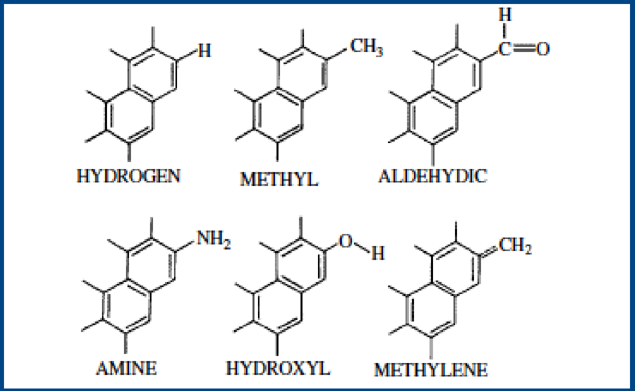

PAHs

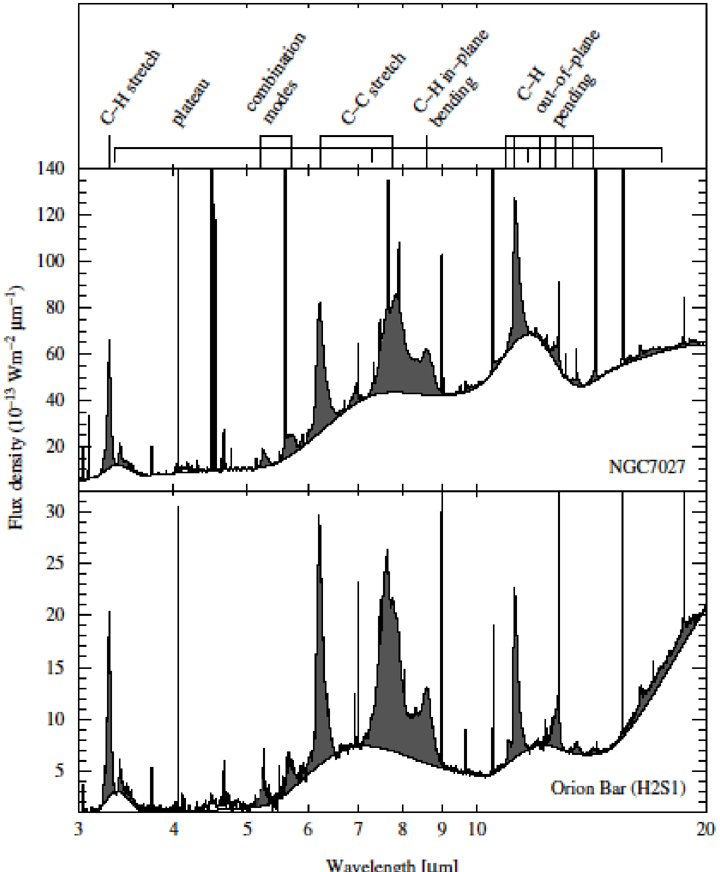

Peeters *et al.* 2004
proceedings *Astrophysics of Dust*

Figure 6.16 The 3–15 μm spectra of the PDRs associated with the Orion Bar and NGC 7027, illustrating the ubiquitous nature as well as the richness of the IR emission features. The IR emission features are shaded. The narrow lines are HI recombination lines, H_2 pure rotational and rotational–vibrational lines, and atomic fine-structure lines. The top panel indicates the PAH vibrational modes associated with each feature. Note the presence of broad plateaus underneath the narrow emission features. Figure adapted from E. Peeters, *et al.*, 2002, *A. & A.*, **390**, p. 1089.

Table 6.5 *The IR emission features and interstellar PAHs*

Band	Assignment
3.3 μm	aromatic C–H stretching mode
3.4 μm	aliphatic C–H stretching mode in methyl groups
	C–H stretching mode in hydrogenated PAHs
	hot band of the aromatic C–H stretch
5.2 μm	combination mode, C–H bend and C–C stretch
5.65 μm	combination mode, C–H bend and C–C stretch
6.0 μm	C–O stretching mode (?)
6.2 μm	aromatic C–C stretching mode
6.9 μm	aliphatic C–H bending modes
7.6 μm	C–C stretching and C–H in-plane bending modes
7.8 μm	C–C stretching and C–H in-plane bending modes
8.6 μm	C–H in-plane bending modes
11.0 μm	C–H out-of-plane bending modes, solo, cation
11.2 μm	C–H out-of-plane bending modes, solo, neutral
12.7 μm	C–H out-of-plane bending modes, trio, cation (?)
13.6 μm	C–H out-of-plane bending modes, quartet
14.2 μm	C–H out-of-plane bending modes, quartet
16.4 μm	in-plane and out-of-plane C–C–C bending modes in pendant ring (?)
Plateaus	
3.2–3.6 μm	overtone and combination modes, C–C stretch
6–9 μm	blend of many C–C stretch and C–H in-plane bend modes[a]
11–14 μm	blend of C–H out-of-plane bending modes[a]
15–19 μm	in-plane and out-of-plane C–C–C bending modes

[a] In PAH clusters

Spitzer data (PAHs and H_2)

Berné et al. (2009), ApJ 706, L160

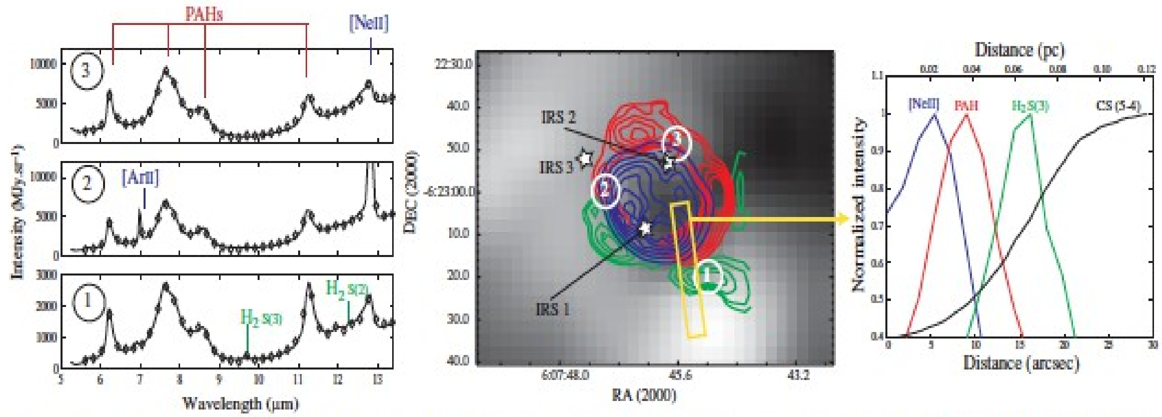

Figure 1. Overview of the Mon R2 region seen with *Spitzer*. Left: observed IRS spectra for PDRs 1, 2, and 3 (continuous line) and fit by the model (diamonds, see Section 4.2.1). Middle: the blue contours represent the intensity of the [Ne II] line (0.02–0.1 erg s^{-1} cm^{-2} sr^{-1} in linear steps), the red contours the intensity of the PAH 11.3 μm band (1.8–3.4 × 10^{-2} erg s^{-1} cm^{-2} sr^{-1} in linear steps), and the green contours the intensity of the H_2 0–0 emission in the *S*(3) rotational line at 9.7 μm ((1.5–4.5) × 10^{-4} erg s^{-1} cm^{-2} sr^{-1} in linear steps). The background map shows the CS *J* = 5–4 emission presented in Choi et al. (2000). Low emission is in black. Numbers indicate the positions of the selected PDRs. Right: cut in the map along the yellow box, showing the stratified emission of the different lines.

Bright, extended emission of the PAHs bands and H_2 rotational lines

Layered structure expected in a PDR

Different PDRs around UCHII region (different physical and chemical conditions)

G_0 and n_H estimates from PAHs and H_2

Table 2
Derived Physical Parameters for PDR 1, PDR 2, and PDR 3

Position	n_H (cm^{-3})	T_{rot}(K)	G_0
PDR 1	$4.3^{\pm0.5} \times 10^5$	574^{+25}_{-22}	$1.6^{\pm0.2} \times 10^5$
PDR 2	$4.0^{\pm0.4} \times 10^4$	331^{+19}_{-17}	$3.3^{\pm0.3} \times 10^4$
PDR 3	$3.7^{\pm0.3} \times 10^4$	314^{+18}_{-16}	$3.7^{\pm0.2} \times 10^4$
Mon R2	$4.0^{\pm0.4} \times 10^4$	321^{+18}_{-16}	$3.7^{\pm0.4} \times 10^4$

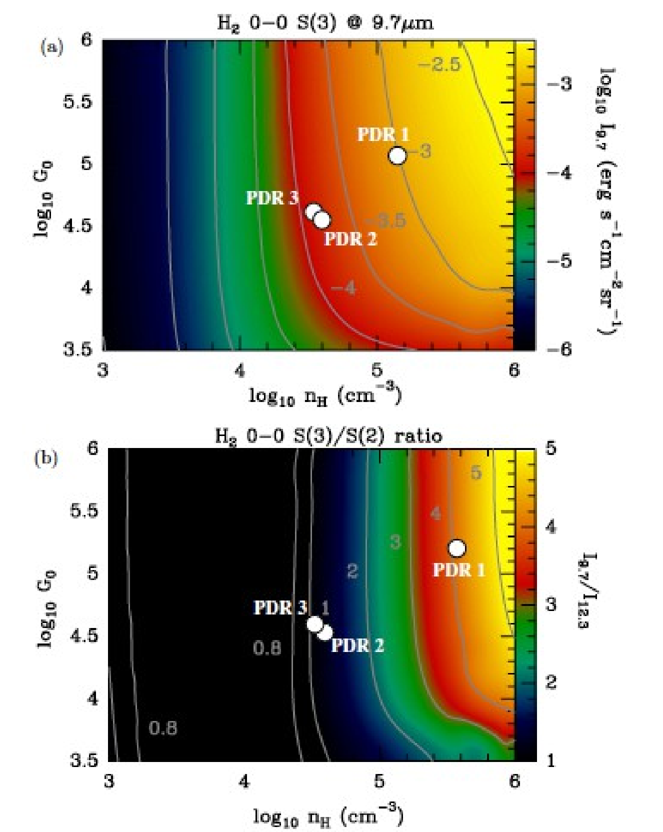

Figure 2. Results from the Meudon PDR code for high UV field/density conditions. (a) Variations of the H_2 0–0 $S(3)$ absolute intensity (colors and contours) as a function of the hydrogen nuclei density n_H and intensity of the radiation field G_0. (b) Variations of the $S(3)/S(2)$ line ratio (colors and contours) as a function of n_H and G_0. Circles indicate the intersection between observed values of $I_{S(3)}$ (panel (a)) and $I_{S(3)}/I_{S(2)}$ (panel (b)) and the G_0 derived using PAH ionization fraction for PDRs 1, 2, and 3.

H_2 rotational lines are thermalized for $n>10^4$ cm^{-3}
The $I_{6.2}/I_{11.3}$ ratio is tracing the $[PAH^+]/[PAH^0]$ ratio and hence the UV field (Galliano et al. 2008).

$$G_0(T/10^3)^{1/2}/n_H \simeq (1990[C]/[H])\times((I_{6.2}/I_{11.3})-0.26).$$

Berné et al. (2009), ApJ 706, L160

ALMA observations of the Orion Bar

Goicoechea et al. (2016), Nature 537, 207

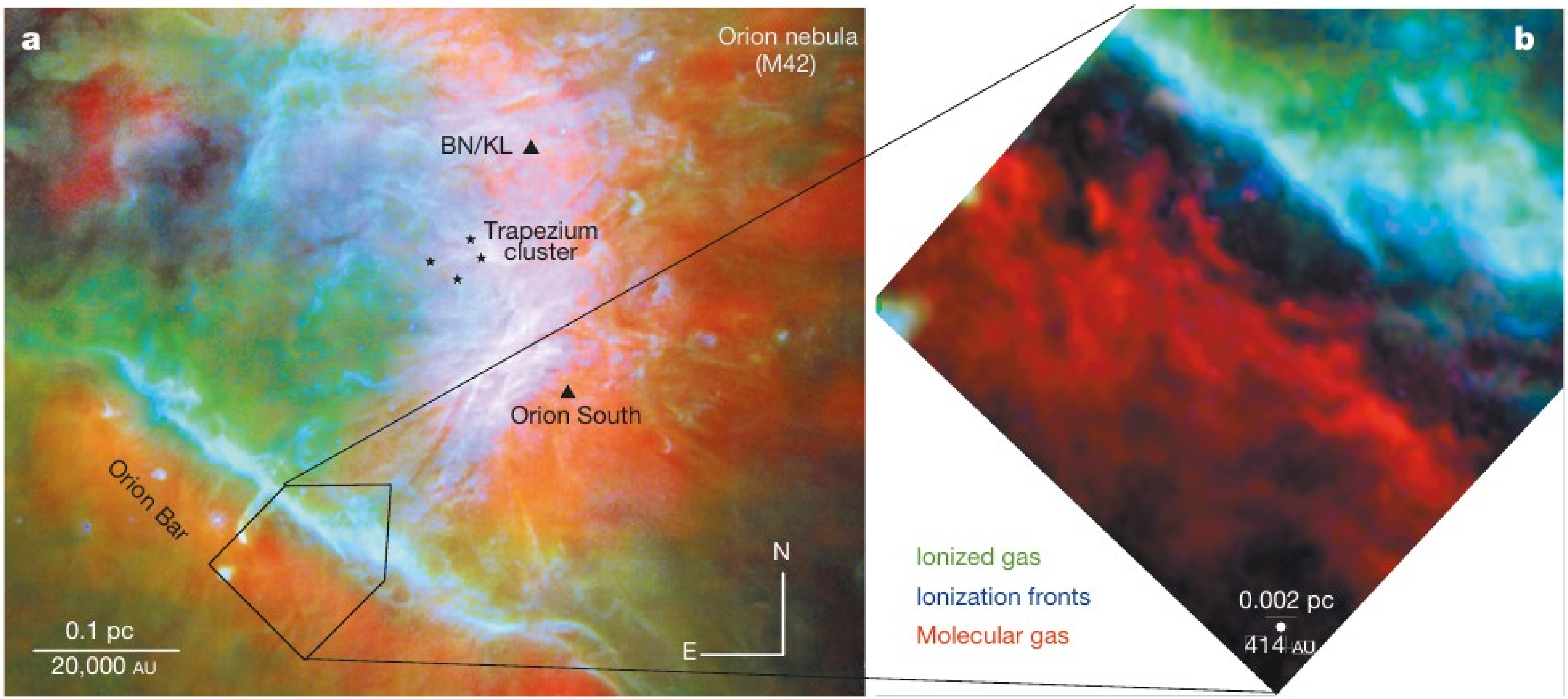

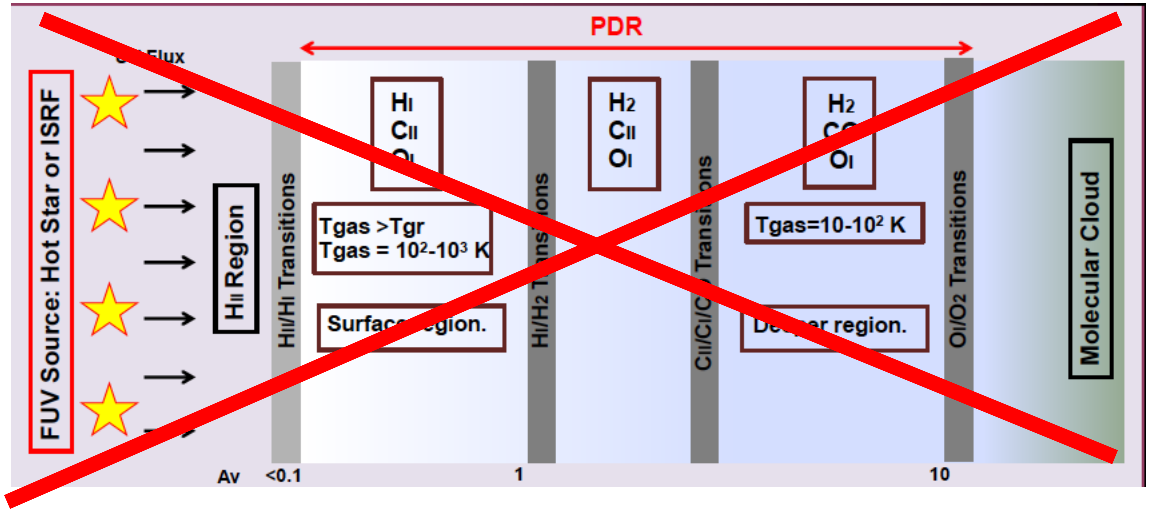

$P_{mol} = P_{ion}$ Equilibrium

$P_{mol} < P_{ion}$ ExpansionI

$P_{mol} > P_{ion}$ Photoevaporation

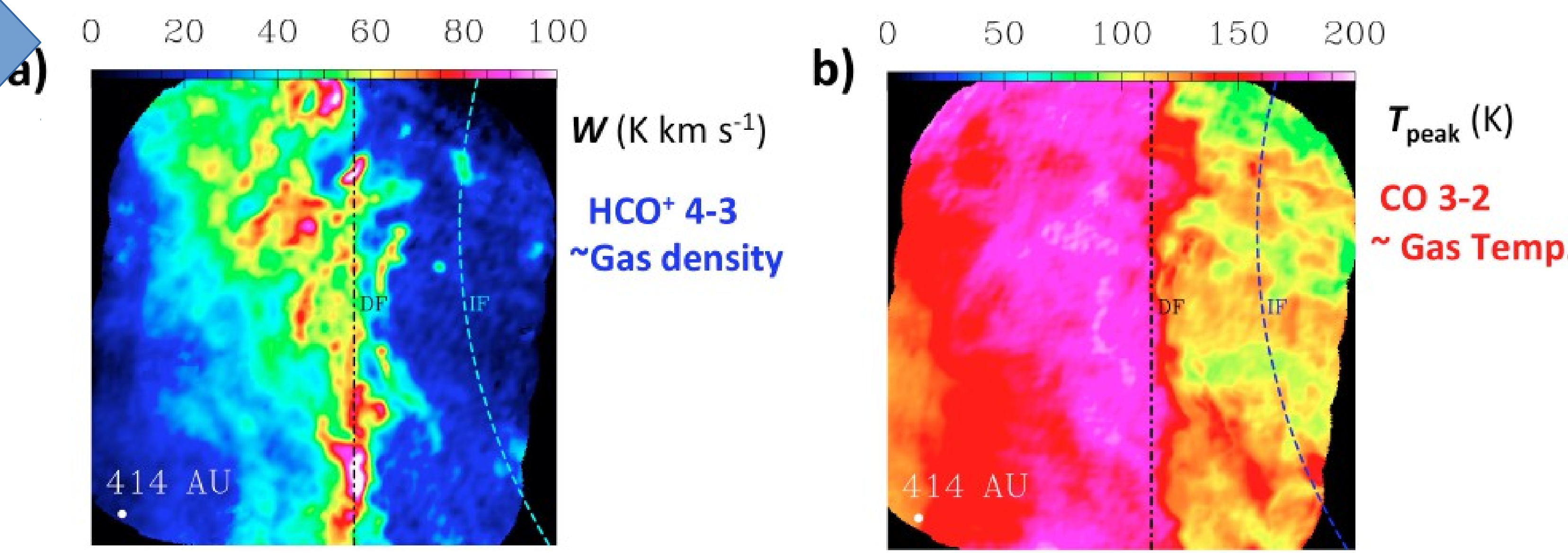

ALMA observations of the Orion Bar

Goicoechea et al. (2016), Nature 537, 207

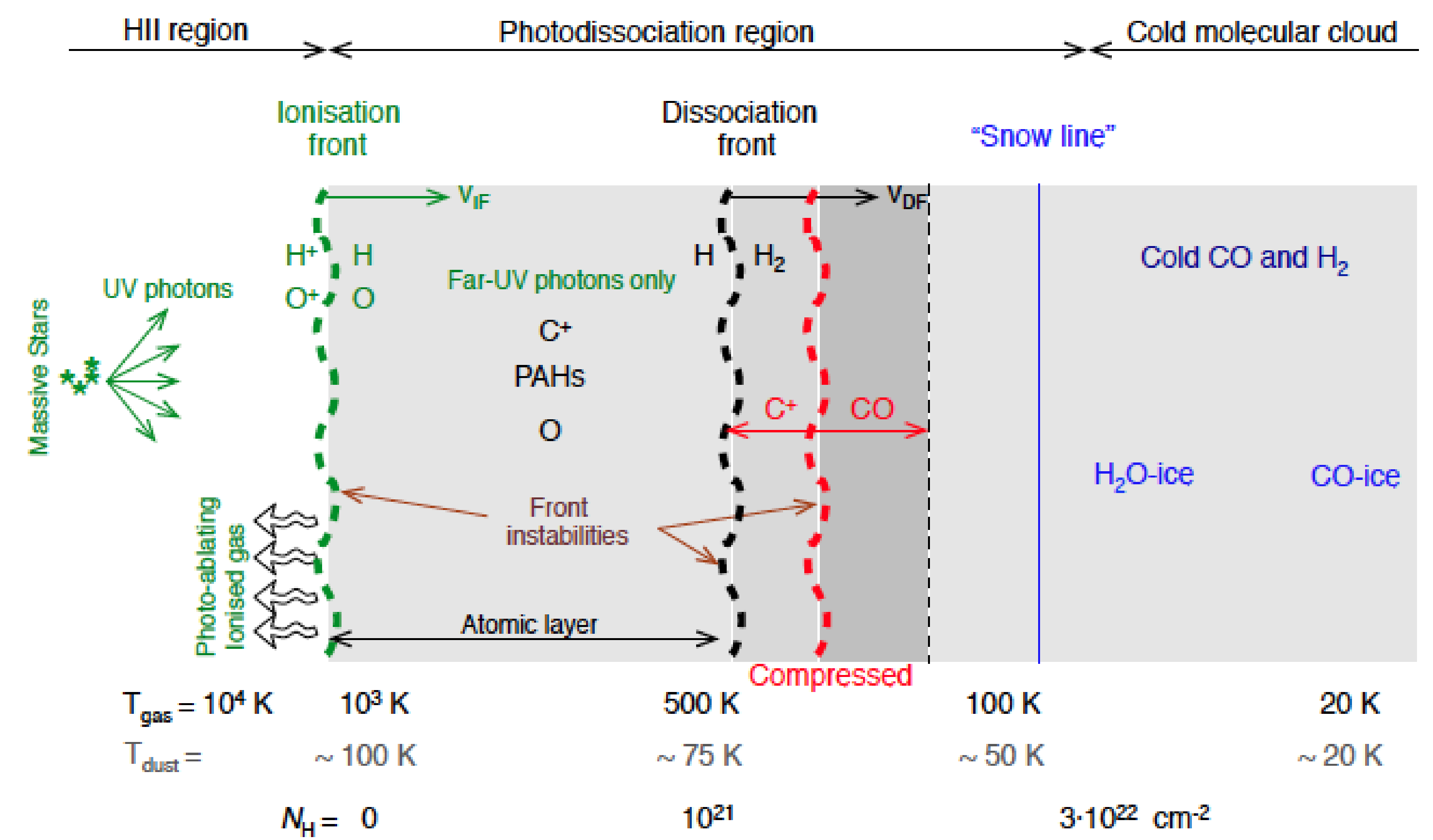

Extended Data Figure 1: Structure of a strongly UV-irradiated molecular cloud edge. The incident stellar UV radiation comes from the left. The velocity of the advancing ionisation and dissociation fronts are represented by v_{IF} and v_{DF} respectively. In the Orion Bar, the dissociation front is at about 15″ (~0.03 pc) from the ionisation front.

Photoevaporating PDR models (the HYDRA core)

Bron et al. (2018), arXiv:1801.01547

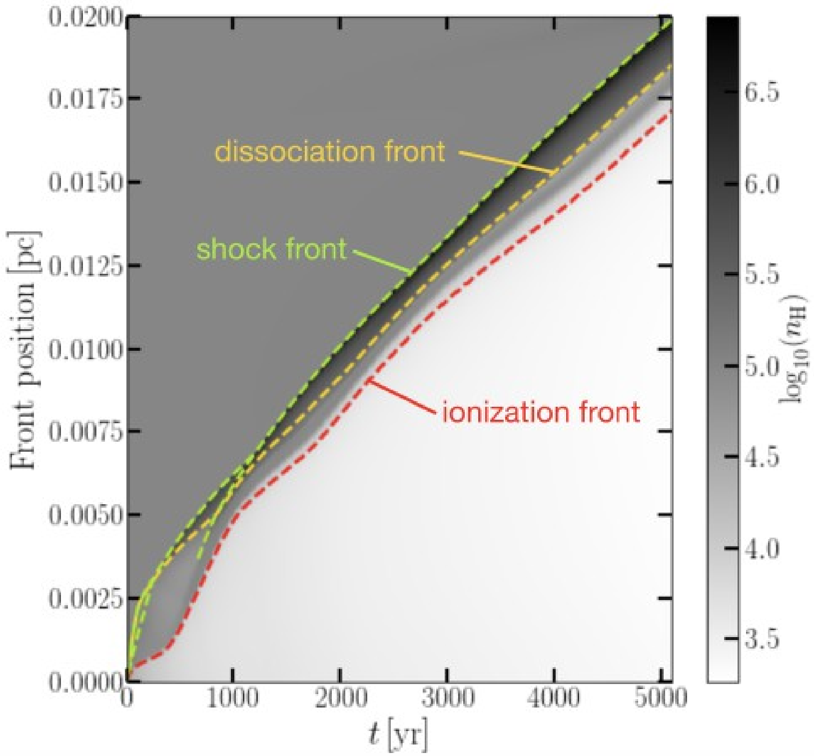

Fig. 8. Evolution of the ionization front position (red dashed line), dissociation front position (yellow dashed line), and shock front position (green dashed line) for the example model $n_0 = 10^5\ \mathrm{cm}^{-3}$, $G_0 = 10^4$, $T_* = 4 \times 10^4$ K, superimposed on the time-position gas density colormap.

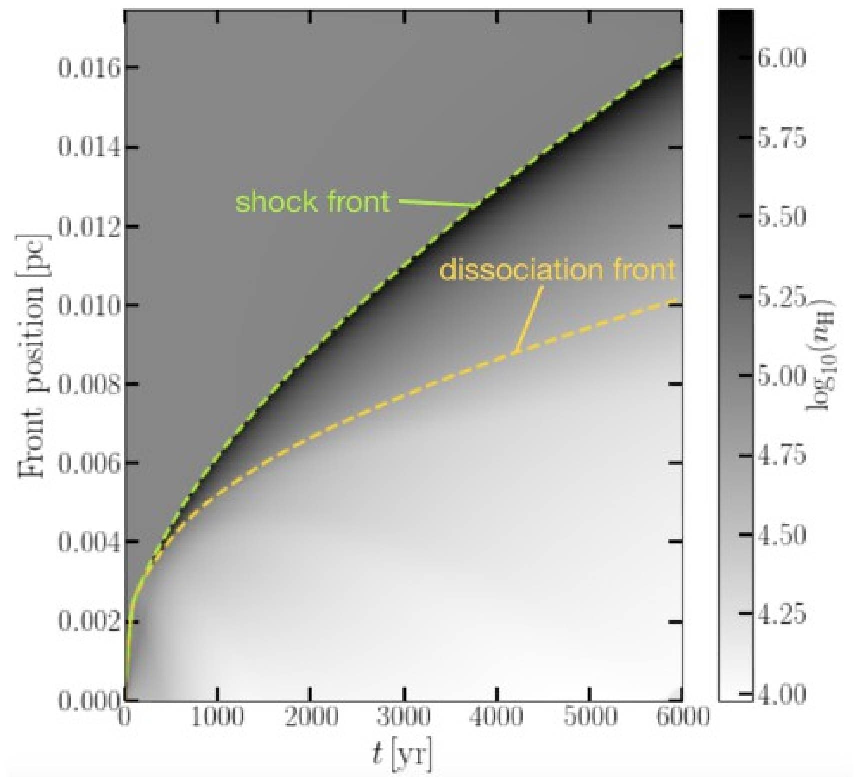

Fig. 11. Evolution of the dissociation front position (yellow dashed line), and shock front position (green dashed line) for the B star example model $n_0 = 10^5\ \mathrm{cm}^{-3}$, $G_0 = 10^4$, $T_* = 1.9 \times 10^4$ K, superimposed on the time-position gas density colormap.

High-J CO emission lines with Herschel

Joblin et al. (2018)arXiv:1801.03893

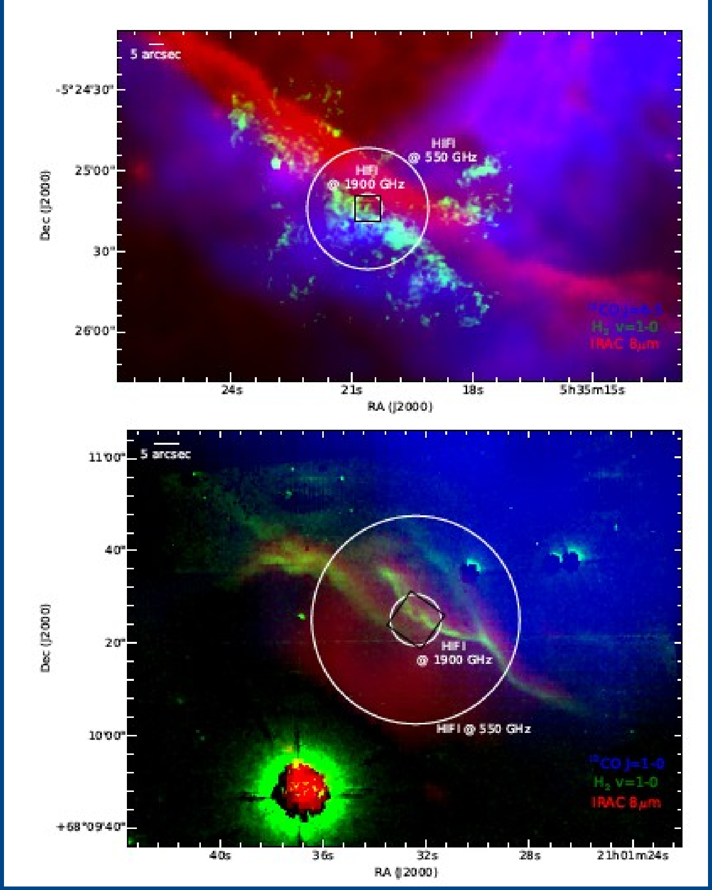

Table 1. Observed data for NGC 7023, and dilution factor Ω. The reported intensities have not been corrected for beam dilution.

Line			Observation data sets [$W m^{-2} sr^{-1}$]				
Species	Transition	Position	SPIRE	HIFI	PACS	others	Ω (dilution factor)
^{12}CO							
	J=4-3	461.041 GHz	$7.6 \pm 2.3 (-10)$	-	-	-	0.05
	J=5-4	576.268 GHz	$2.0 \pm 0.6 (-9)$	-	-	-	0.07
	J=6-5	691.473 GHz	$5.3 \pm 1.6 (-9)$	$7.5 \pm 0.7 (-9)$	-	-	0.08
	J=7-6	806.652 GHz	$1.1 \pm 0.3 (-8)$	-	-	-	0.10
	J=8-7	921.800 GHz	$1.1 \pm 0.3 (-8)$	$2.5 \pm 0.3 (-8)$	-	-	0.11
	J=9-8	1036.912 GHz	$1.8 \pm 0.5 (-8)$	$4.2 \pm 0.4 (-8)$	-	-	0.12
	J=10-9	1151.985 GHz	$1.9 \pm 0.6 (-8)$	$3.5 \pm 0.4 (-8)$	-	-	0.14
	J=11-10	1267.014 GHz	$2.8 \pm 0.8 (-8)$	-	-	-	0.15
	J=12-11	1381.995 GHz	$2.5 \pm 0.7 (-8)$	-	-	-	0.17
	J=13-12	1496.923 GHz	$2.5 \pm 0.7 (-8)$	$3.9 \pm 0.5 (-8)$	-	-	0.18
	J=15-14	1726.603 GHz	-	-	$3.4 \pm 0.7 (-8)$	-	0.21
	J=16-15	1841.345 GHz	-	-	$2.0 \pm 0.4 (-8)$	-	0.23
	J=17-16	1956.018 GHz	-	-	$1.2 \pm 0.3 (-8)$	-	0.28
	J=18-17	2070.616 GHz	-	-	$7.3 \pm 1.7 (-9)$	-	0.28
	J=19-18	2185.135 GHz	-	-	$4.3 \pm 2.5 (-9)$	-	0.28
^{13}CO							
	J=5-4	550.926 GHz	$1.0 \pm 0.3 (-9)$	$1.7 \pm 0.2 (-9)$	-	-	0.07
	J=6-5	661.067 GHz	$1.1 \pm 0.3 (-9)$	-	-	-	0.08
	J=7-6	771.184 GHz	$1.8 \pm 0.5 (-9)$	-	-	-	0.09
	J=8-7	881.273 GHz	$2.3 \pm 0.7 (-9)$	$4.1 \pm 0.4 (-9)$	-	-	0.11
	J=9-8	991.329 GHz	$3.8 \pm 1.1 (-9)$	-	-	-	0.12
	J=10-9	1101.350 GHz	$3.1 \pm 0.9 (-9)$	$4.8 \pm 0.5 (-9)$	-	-	0.13
CH^+							
	J=1-0	835.137 GHz	-	$1.0 \pm 0.1 (-9)$	-	-	0.10
	J=2-1	1669.281 GHz	-	$5.5 \pm 0.8 (-9)$	$6.6 \pm 2.5 (-9)$	-	0.28
	J=3-2	2501.440 GHz	-	-	$5.6 \pm 2.1 (-9)$	-	0.28
HCO^+							
	J=1-0	89.188 GHz	-	-	-	$4.5 \pm 1.3 (-12)^a$	0.49
	J=6-5	535.062 GHz	-	$8.2 \pm 0.7 (-11)$	-	-	0.06
C^+							
	$^2P_{3/2}$ - $^2P_{1/2}$	157.68 μm	-	$7.6 \pm 1.1 (-7)$	$7.3 \pm 1.5 (-7)$	$9.9 \pm 2.0 (-7)^b$	0.28
C							
	$^3P_1$ - $^3P_0$	492.161 GHz	$2.8 \pm 0.8 (-10)$	-	-	-	0.10
O							
	$^3P_0$ - $^3P_1$	145.53 μm	-	-	$4.0 \pm 0.8 (-7)$	$3.8 \pm 0.8 (-7)^b$	0.28
	$^3P_1$ - $^3P_2$	63.18 μm	-	-	-	$1.8 \pm 0.4 (-6)^b$	0.28
HD							
	J=0-1	112.07 μm	-	-	$2.7 \pm 2.2 (-9)$	-	0.28
H_2			ISO-SWS	Spitzer	CFHT [c]	Perkins Telescope[d]	-
	0-0 S(0)	28.22 μm	$3.4 \pm 1.0 (-8)$	-	-	-	0.10
	0-0 S(1)	17.03 μm	$2.1 \pm 0.4 (-7)$	$2.0^{+0.6}_{-0.3} (-7)$	-	-	0.10^{ISO} / $0.20^{Spitzer}$
	0-0 S(2)	12.28 μm	$2.4 \pm 0.6 (-7)$	$5.5^{+2.0}_{-1.7} (-7)$	-	-	0.10^{ISO} / $0.55^{Spitzer}$
	0-0 S(3)	9.66 μm	$4.1 \pm 1.0 (-7)$	$6.9^{+3.1}_{-1.5} (-7)$	-	-	0.10^{ISO} / $0.55^{Spitzer}$
	0-0 S(4)	8.02 μm	$1.5 \pm 0.4 (-7)$	-	-	-	0.10^{ISO} / $0.55^{Spitzer}$
	0-0 S(5)	6.91 μm	$2.6 \pm 0.4 (-7)$	$4.6 \pm 1.4 (-7)$	-	-	0.10^{ISO} / $0.55^{Spitzer}$
	1-0 S(1)	2.12 μm	-	-	$2.1 \pm 0.21 (-7)$	-	1
	1-0 S(2)	2.03 μm	-	-	$7.6 \pm 1.7 (-8)$	-	1
	2-1 S(1) / 1-0 S(1)		-	-	-	0.29	

[a] Fuente et al. (1996) - [b] Bernard-Salas et al. (2015) - [c] Lemaire et al. 1996, 1999 - [d] Martini et al. 1999

High-J CO emission lines with Herschel

Joblin et al. (2018)arXiv:1801.03893

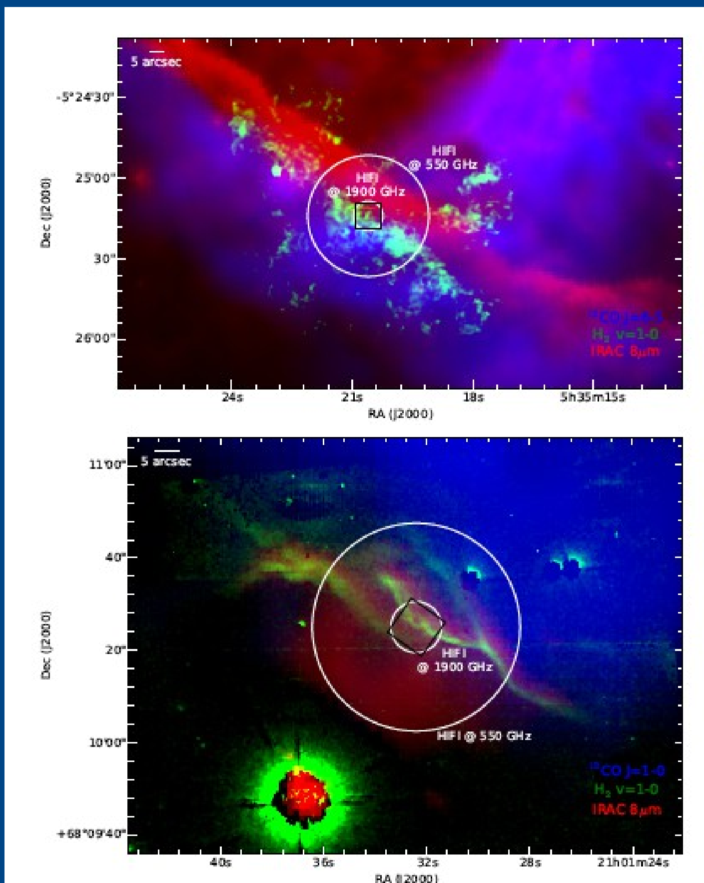

Table 2. Observed data for the Orion Bar and dilution factor Ω. The reported intensities have not been corrected for beam dilution.

Line			Integrated intensity [$\mathrm{W\,m^{-2}\,sr^{-1}}$]				
Species	Transition	Position	SPIRE	HIFI	PACS	others	Ω
^{12}CO							
	J=4-3	461.041 GHz	1.5 ± 0.5 (−8)	-	-	-	0.05
	J=5-4	576.268 GHz	3.7 ± 1.1 (−8)	7.0 ± 0.6 (−8)	-	-	0.07
	J=6-5	691.473 GHz	7.2 ± 2.2 (−8)	1.2 ± 0.1 (−7)	-	-	0.08
	J=7-6	806.652 GHz	1.5 ± 0.5 (−7)	1.8 ± 0.2 (−7)	-	-	0.10
	J=8-7	921.800 GHz	1.7 ± 0.5 (−7)	2.7 ± 0.3 (−7)	-	-	0.11
	J=9-8	1036.912 GHz	3.1 ± 0.9 (−7)	3.3 ± 0.3 (−7)	-	-	0.12
	J=10-9	1151.985 GHz	3.6 ± 1.1 (−7)	3.5 ± 0.5 (−7)	-	-	0.14
	J=11-10	1267.014 GHz	4.1 ± 1.2 (−7)	4.4 ± 0.6 (−7)	-	-	0.15
	J=12-11	1381.995 GHz	4.2 ± 1.3 (−7)	-	-	-	0.17
	J=13-12	1496.923 GHz	3.9 ± 1.2 (−7)	4.8 ± 0.7 (−7)	-	-	0.18
	J=14-13	1611.793 GHz	-	5.1 ± 0.7 (−7)	4.3 ± 0.9 (−7)	-	0.20
	J=15-14	1726.603 GHz	-	5.1 ± 0.7 (−7)	4.4 ± 0.9 (−7)	-	0.21
	J=16-15	1841.345 GHz	-	3.3 ± 0.5 (−7)	3.7 ± 0.7 (−7)	-	0.23
	J=17-16	1956.018 GHz	-	-	2.8 ± 0.6 (−7)	-	0.28
	J=18-17	2070.616 GHz	-	-	1.4 ± 0.3 (−7)	-	0.28
	J=19-18	2185.135 GHz	-	-	9.1 ± 1.8 (−8)	1.1 ± 0.2 (−7)[a]	0.28
	J=20-19	2299.570 GHz	-	-	6.2 ± 1.3 (−8)	-	0.28
	J=21-20	2413.917 GHz	-	-	2.8 ± 0.7 (−8)	-	0.28
	J=23-22	2642.330 GHz	-	-	1.8 ± 0.6 (−8)	-	0.28
^{13}CO							
	J=5-4	550.926 GHz	7.5 ± 2.2 (−9)	*1.5 ± 0.1 (−8)	-	-	0.07
	J=6-5	661.067 GHz	1.9 ± 0.6 (−8)	-	-	-	0.08
	J=7-6	771.184 GHz	3.3 ± 1.0 (−8)	4.0 ± 0.4 (−8)	-	-	0.09
	J=8-7	881.273 GHz	4.2 ± 1.3 (−8)	4.8 ± 0.5 (−8)	-	-	0.11
	J=9-8	991.329 GHz	5.1 ± 1.5 (−8)	4.9 ± 0.5 (−8)	-	-	0.12
	J=10-9	1101.350 GHz	4.3 ± 1.3 (−8)	5.6 ± 0.6 (−8)	-	-	0.13
	J=11-10	1211.330 GHz	4.0 ± 1.2 (−8)	4.6 ± 0.6 (−8)	-	-	0.15
	J=12-11	1321.265 GHz	3.1 ± 0.9 (−8)	-	-	-	0.16
	J=13-12	1431.153 GHz	2.0 ± 0.6 (−8)	-	-	-	0.17
	J=15-14	1650.767 GHz	-		7.6 ± 2.2 (−9)	-	0.20
	J=16-15	1760.486 GHz	-	-	4.4 ± 2.5 (−9)	-	0.22
CH^+							
	J=1-0	835.137 GHz	-	1.30 ± 0.13 (−8)	-	-	0.10
	J=2-1	1669.281 GHz	-	4.32 ± 0.60 (−8)	-	-	0.28
	J=3-2	2501.440 GHz	-	-	3.4 ± 0.8 (−8)	-	0.28
	J=4-3	3330.630 GHz	-	-	3.3 ± 0.8 (−8)	-	0.28
	J=5-4	4155.872 GHz	-	-	2.8 ± 1.0 (−8)	-	0.28
	J=6-5	4976.201 GHz	-	-	1.9 ± 1.1 (−8)	-	0.28
OH							
	$^2\Pi_{3/2}\ J = 5/2^+ - 3/2^-$	119.4416 μm	-	-	7.8 ± 1.6 (−8)	-	0.28
	$^2\Pi_{3/2}\ J = 5/2^- - 3/2^+$	119.2345 μm	-	-	6.6 ± 1.4 (−8)	-	0.28
	$^2\Pi_{1/2} -^2\Pi_{3/2}\ J = 1/2^+ - 3/2^-$	79.1792 μm	-	-	6.0 ± 2.2 (−8)	-	0.28
	$^2\Pi_{1/2} -^2\Pi_{3/2}\ J = 1/2^- - 3/2^+$	79.1712 μm	-	-	6.6 ± 2.3 (−8)	-	0.28
	$^2\Pi_{1/2}\ J = 3/2^- - 1/2^+$	163.3962 μm	-	-	1.4 ± 0.3 (−8)	-	0.28
	$^2\Pi_{1/2}\ J = 3/2^+ - 1/2^-$	163.0153 μm	-	-	1.3 ± 0.3 (−8)	-	0.28
	$^2\Pi_{3/2}\ J = 7/2^- - 5/2^+$	84.5967 μm	-	-	3.1 ± 0.9 (−8)	-	0.28
	$^2\Pi_{3/2}\ J = 7/2^+ - 5/2^-$	84.4203 μm	-	-	3.4 ± 1.0 (−8)	-	0.28
	$^2\Pi_{3/2}\ J = 9/2^+ - 7/2^-$	65.2789 μm	-	-	0.5 ± 0.7 (−8)	-	0.28
	$^2\Pi_{3/2}\ J = 9/2^- - 7/2^+$	65.1318 μm	-	-	1.3 ± 0.7 (−8)	-	0.28
HD							
	J=1-0	112.07 μm	-	-	0 ± 4.0 (−9)	-	0.28
	J=2-1	56.23 μm	-	-	3.1 ± 1.1 (−8)	-	0.28
C^+							
	$^2P_{3/2}$ - $^2P_{1/2}$	157.68 μm	-	5.5 ± 0.8 (−6)	-	7.5 ± 1.5 (−6)[b]	0.28
C							
	$^3P_1$ - $^3P_0$	492.161 GHz	-	2.9 ± 0.3(−9)	-	-	0.10
	$^3P_2$ - $^3P_1$	809.342 GHz	-	2.3 ± 0.2(−9)	-	-	0.06
O							
	$^3P_0$ - $^3P_1$	145.53 μm	-	-	-	6.0 ± 1.2 (−6)[b]	0.28
	$^3P_1$ - $^3P_2$	63.18 μm	-	-	5.4 ± 1.1 (−5)	5.0 ± 1.0 (−5)	0.28
H_2			ISO SWS[c]	IRTF[d]	CFHT[e]		
	0-0 S(0)	28.22 μm	0.9 ± 0.3 (−7)	-	-		0.10
	0-0 S(1)	17.03 μm	6.5 ± 1.3 (−7)	8.5 ± 0.3 (−7)	-		0.10
	0-0 S(2)	12.28 μm	3.7 ± 0.9 (−7)	6.8 ± 0.2 (−7)	-		0.10
	0-0 S(3)	9.66 μm	6.0 ± 1.5 (−7)	-	-		0.10
	0-0 S(4)	8.02 μm	2.8 ± 0.7 (−7)	4.1 ± 0.2 (−7)	-		0.10
	0-0 S(5)	6.91 μm	6.4 ± 1 (−7)	-	-		0.10
	1-0 S(1)	2.12 μm		-	5.8 (−7)	3.6(−7)[f]	1
	2-1 S(1)	2.25 μm		-	1.2 (−7)		1

[a]Parikka et al. (2017). [b]Bernard Salas et al. (2012) - [c] Bertoldi,private comm., Habart et al. (2004) - [d]Allers et al. (2005) - [e] Joblin, Maillard, Noel, unpublished BEAR data - [f] van der Werf (1996).

Photoevaporating PDR models (the HYDRA core)

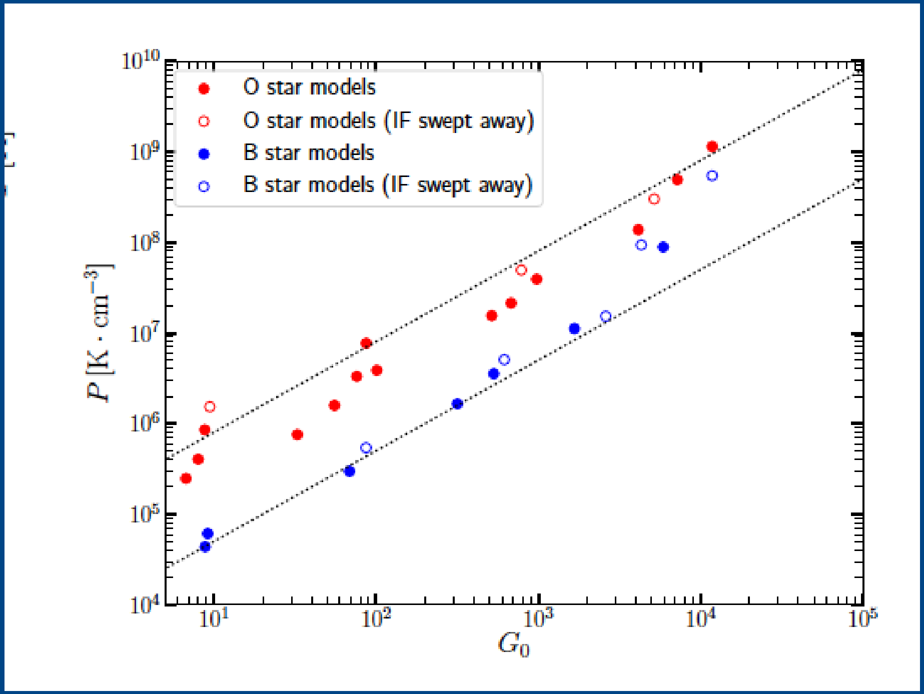

Bron et al. (2018), arXiv:1801.01547

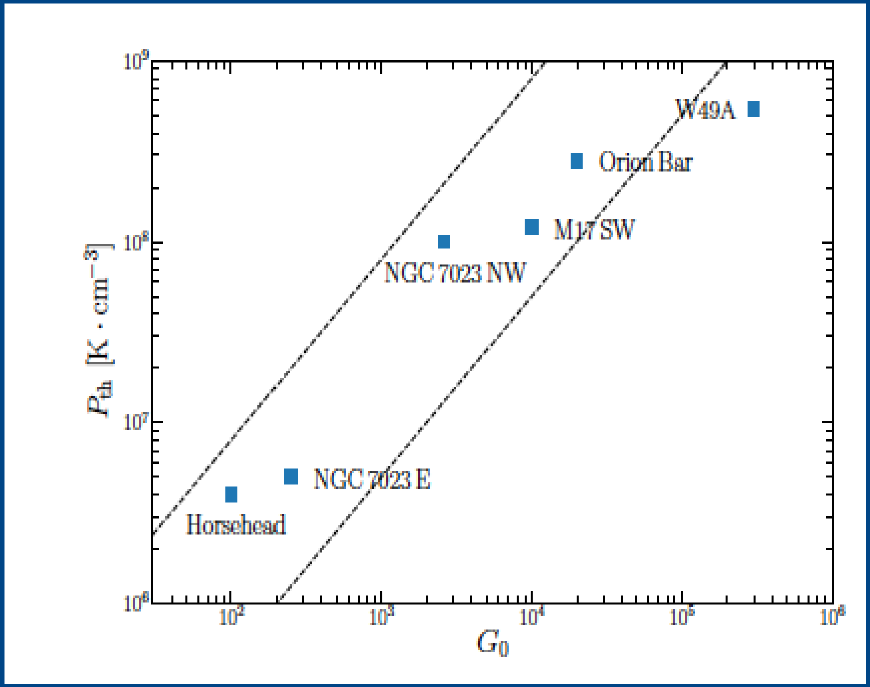

Joblin et al. (2018)arXiv:1801.03893

References

1.- “The Physics and Chemistry of the Interstellar Medium”, A.G.G.M. Tielens, de. Cambridge University Press

2.- Tielens, A.G.G.M. & Hollenbach, D. J., 1985, ApJ 291, 722

3.- Hollenbach, D. J., Takahashi, T., Tielens, A.G.G.M. 1985, ApJ 291, 722